ROYAL SOCIETY OPEN SCIENCE

royalsocietypublishing.org/journal/rsos

Research

Cite this article: de los Reyes V AA, Kim Y. 2022 Optimal regulation of tumour-associated neutrophils in cancer progression. *R. Soc. Open Sci.* **9**: 210705.
https://doi.org/10.1098/rsos.210705

Received: 10 June 2021
Accepted: 19 November 2021

Subject Category:
Mathematics

Subject Areas:
computational biology/mathematical modelling

Keywords:
tumour-associated neutrophils, TGF-beta, IFN-beta, optimal control, tumour growth, mathematical model

Author for correspondence:
Yangjin Kim
e-mail: ahyouhappy@gmail.com

Optimal regulation of tumour-associated neutrophils in cancer progression

Aurelio A. de los Reyes V[1,2] and Yangjin Kim[3,4]

[1]Biomedical Mathematics Group, Pioneer Research Center for Mathematical and Computational Sciences, Institute for Basic Science, Daejeon 34126, Republic of Korea
[2]Institute of Mathematics, University of the Philippines Diliman, Quezon City 1101, Philippines
[3]Department of Mathematics, Konkuk University, Seoul 05029, Republic of Korea
[4]Mathematical Biosciences Institute, Columbus, OH 43210, USA

AAdlRV, 0000-0001-5418-4579; YK, 0000-0002-8905-8481

In a tumour microenvironment, tumour-associated neutrophils could display two opposing differential phenotypes: anti-tumour (N1) and pro-tumour (N2) effector cells. Converting N2 to N1 neutrophils provides innovative therapies for cancer treatment. In this study, a mathematical model for N1-N2 dynamics describing the cancer survival and immune inhibition in response to TGF-β and IFN-β is considered. The effects of exogenous intervention of TGF-β inhibitor and IFN-β are examined in order to enhance N1 recruitment to combat tumour progression. Our approach employs optimal control theory to determine drug infusion protocols that could minimize tumour volume with least administration cost possible. Four optimal control scenarios corresponding to different therapeutic strategies are explored, namely, TGF-β inhibitor control only, IFN-β control only, concomitant TGF-β inhibitor and IFN-β controls, and alternating TGF-β inhibitor and IFN-β controls. For each scheme, different initial conditions are varied to depict different pathophysiological condition of a cancer patient, leading to adaptive treatment schedule. TGF-β inhibitor and IFN-β drug dosages, total drug amount, infusion times and relative cost of drug administrations are obtained under various circumstances. The control strategies achieved could guide in designing individualized therapeutic protocols.

1. Introduction

Cancer is the leading cause of death worldwide [1,2]. Various immune cells including neutrophils [3], natural killer (NK) cells [4] and macrophages [5] in tumour microenvironment (TME) play a major role in regulation of tumour growth and

THE ROYAL SOCIETY PUBLISHING

anti-tumour treatment in many cancers including lung cancers. Copious neutrophils in the blood constitute the first protection in innate immunity [6,7]. Approximately 10^{11} neutrophils are generated in the bone marrow and released into the blood circulation every day [8]. Neutrophil recruitment at sites of infection or injury is triggered by the release of pathogen- or damage-associated molecular patterns from invading microorganisms or damaged and/or dead cells, respectively [9]. The process of neutrophil extravasation comprises a complex multistep cascade that is tightly regulated by coordinated sequence of adhesive and migratory events [6,10]. Neutrophils undergo a series of mechanisms, including phagocytosis, and the development and regulation of neutrophil extracellular traps (NETs) [11]. Furthermore, neutrophils release proteinases into the surrounding tissue damaging the host [12], and produce cytokines and chemokines influencing inflammatory and immune responses [13,14].

Aside from the traditional antimicrobial functions, there is increasing evidence suggesting that tumour-associated neutrophils (TANs) play a major role in tumour progression from formation to malignant state [15–19]. Several clinical and laboratory studies have indicated that the presence of TANs has been assessed with poor prognosis in various tumours including metastatic melanoma [20], bronchoalveolar carcinoma [21], renal carcinoma [22], and head and neck squamous cell carcinoma (HNSCC) [23]. In these conditions, neutrophils exhibit a pro-tumour phenotype which is detrimental to the host. TME controls neutrophil recruitment and thus, TANs promote tumour progression. Hence, TANs display two differential phenotypes [15,16,24]: (i) an anti-tumourigenic role (called N1), and (ii) pro-tumour progression (called N2).

There is mounting evidence that the immunosuppressive cytokine TGF-β skews neutrophil differentiation towards N2 phenotype [24–26], while TGF-β inhibitor and type-1 IFN (α, β, ω) therapy are recognized to alter neutrophils toward the N1 phenotype [27,28]. Several studies have shown that IFN-β in tumour microenvironment interacts with key molecules in signalling pathways activating its functions to stimulate anti-tumour activities [29–32]. Therefore, normalization of TME by the N2→N1 transition can lead to better control of tumour growth. For example, injection of IFN-β [29,31,33–35] or TGF-β inhibitor such as galunisertib [36–40] and LY2109761 [41,42] can be a novel anti-tumour strategy due to their effective tumour killing and anti-tumour immune response [43,44].

Mathematical modelling is a valuable tool in providing information to understand the complex mechanisms and processes in cancer [45,46]. Models can generate theories and hypotheses on quantitative grounds and provide reasonable predictions that could aid scientists towards the next series of experiments [47]. Furthermore, mathematical modelling can help clinicians to evaluate tumour microenvironment and develop anti-tumour strategies [48–52]. In addition, *in silico* models could play a significant role in optimizing clinical trial design and patient stratification, suggesting different treatment modalities, and alter risk prognoses [53–59].

In this work, we consider the following variables in a mathematical model:

$$\begin{aligned} C(t) &= \text{density of the N2 complex at time } t;\\ I(t) &= \text{density of the N1 complex at time } t;\\ T(t) &= \text{tumour volume at time } t;\\ G(t) &= \text{concentration of TGF-}\beta \text{ at time } t;\\ L(t) &= \text{concentration of TGF-}\beta \text{ inhibitor at time } t;\\ S(t) &= \text{concentration of IFN-}\beta \text{ at time } t; \end{aligned}$$

In this study, regulation of N1 and N2 TANs is explored through TGF-β inhibitor and IFN-β controls in the framework of optimal control theory having the objective of minimizing the tumour size with least drug administration cost. In particular, infusion scheme(s) accounting for the amount and frequency of administration is explored. Various initial N1 and N2 phenotypes are also considered to simulate individualized therapeutic regimen depending on current pathological conditions. Several control strategies including combination therapies are examined under different circumstances that could give the best clinical outcomes.

We found therapeutic regimen at regulating anti- and pro-tumoural neutrophil phenotypic states by means of four different administration modalities of a TGF-β inhibitor and IFN-β cytokine in lung cancer. The optimal control strategy predicts that, depending on pathological states, therapies may have to be adjusted accordingly to minimize adverse effects of drugs and its administration cost.

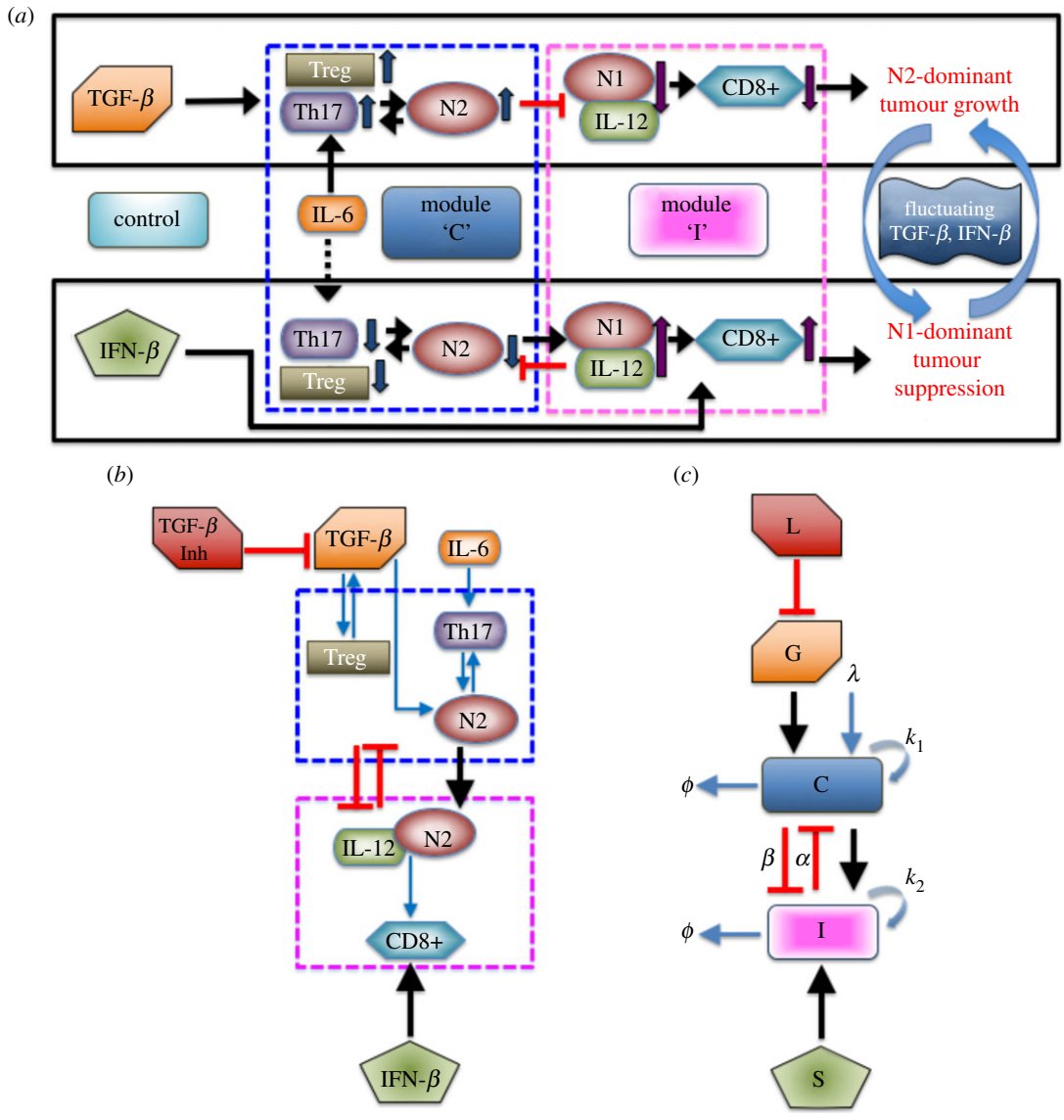

Figure 1. (*a*) N1 and N2 complexes regulate cancer survival and immune inhibition in the presence of TGF-β and IFN-β [60]. (*b*) Simplified model diagram of N1-N2 network dynamics with the inclusion of a TGF-β inhibitor acting as a control to the signalling pathway. (*c*) Schematic non-dimensional model including a TGF-β inhibitor (modified from [60]). Optimal control is applied to obtain appropriate L and S dosages that minimize the tumour volume with minimal costs.

2. Methodology

2.1. Mathematical model

In order to understand the mutual interactions between a tumour and immune system involving tumour-associated neutrophils, a mathematical model of the signalling pathway for lung cancer is proposed in [60]. It consists of the basic network of interactions between cells, cytokines and growth factors. It was shown that IFN-β and TGF-β play a crucial function as tumour suppressor and tumour promoter (refer to figure 1*a*). High levels of TGF-β and low activities of IFN-β induce Treg infiltration generating inhibition of overall anti-tumour immune response of T cells. In addition, TGF-β alters the tumour microenvironment inducing polarization of neutrophil N1 into N2 type while IFN-β can polarize the N2 phenotype back to N1 phenotype [15,61]. The N2-dominant microenvironment contributes to enhance tumour growth. On the contrary, low TGF-β and high IFN-β levels reduce the neutrophil polarization toward N2 from N1 phenotype and enhance immune activities of T cells and N1 TANs, driving tumour suppression. For model simplification, the N2 regulatory network among Treg, Th17 and N2 cells is merged into one

Table 1. Parameters used in the model.

parameter	description	value	references
λ	source (IL-6) term in the N2 component	0.01	[60,62]
G	source (TGF-β) term in the N2 component	0–1.0	[60,63]
k_1	self-regulation rate in the N2 component	4.0	[60]
k_3	scaling parameter	1.0	[60]
α	suppression rate of the N2 component by the N1 component	1.5	[60]
k_2	self-regulation rate in the N1 component	4.0	[60]
k_4	scaling parameter	1.0	[60]
β	suppression rate of the N1 component by the N2 component	1.0	[60]
S	source (IFN-β) term in the N1 component	0.2	[60,64]
μ	decay rate of the N1 component	1.0	[65,66]
C_{th}	threshold (N2 component)	1.81	[60]
I_{th}	threshold (N1 component)	1.29	[60]
r	growth rate of tumour cells	0.05	[33]
K	scaling constant	1.0	[33]
γ_1	suppression strength in immune-mediated growth	0.1	[33]
T_0	carrying capacity of cancer cells	100	[33]
G_S	source term in the TGF-β component	0.826	[60]
μ_G	decay rate (TGF-β)	0.826	[5,67–69]
γ_L	degradation rate of TGF-β through the inhibitor	100	[60]
μ_L	decay rate (TGF-β inhibitor)	6.6	[36]
μ_S	decay rate (IFN-β)	3.96	[70]

component denoted as N2 complex. On the other hand, the immunoregulatory system composed of N1 cells, interleukin IL-12 and CD8+, is incorporated into N1 complex. Further details of model development can be found in [60]. The associated dimensionless equations for complexes N2 (C), N1 (I) and tumour volume (T) is described by the following ordinary differential equations [60]:

$$\left.\begin{aligned}
\frac{\mathrm{d}C}{\mathrm{d}t} &= \underbrace{\lambda}_{\text{source (IL}-6)} + \underbrace{\lambda_G G}_{\text{source (TGF-}\beta)} + \underbrace{\frac{k_1}{k_3^2 + \alpha I^2}}_{\text{inhibition from N1}} - \underbrace{C}_{\text{decay}},\\
\frac{\mathrm{d}I}{\mathrm{d}t} &= \underbrace{\lambda_S S}_{\text{source (IFN-}\beta)} + \underbrace{\frac{k_2}{k_4^2 + \beta C^2}}_{\text{inhibition from N2}} - \underbrace{\mu I}_{\text{decay}}\\
\text{and}\quad \frac{\mathrm{d}T}{\mathrm{d}t} &= \underbrace{r\left(1 + \frac{C}{K + \gamma_1 I}\right) T\left(1 - \frac{T}{T_0}\right)}_{\text{growth}} - \underbrace{\delta I T}_{\text{killing}},
\end{aligned}\right\} \tag{2.1}$$

with essential set of parameters listed in table 1. Here, two sources (IL-6, TGF-β) of the N2 complex are represented in the first and second terms in equation of C while the IFN-β-mediated source of the N1 complex is provided in the first term in equation of I. The third term in equation of C and second term in equation of I represent the mutual inhibition between N1 and N2, respectively. Tumour growth and N1-mediated tumour cell killing are represented in the first and second terms in equation of T, respectively. Finally, the decay process of the N1 and N2 complexes is represented in the last terms in equations of I and C, respectively.

The basic dynamics of the model (2.1) is illustrated in figure 2. Different levels of TGF-β (G) signals could induce either a single stable steady state $\text{SS}^{(s)}$ or three steady states of which two are stable and one

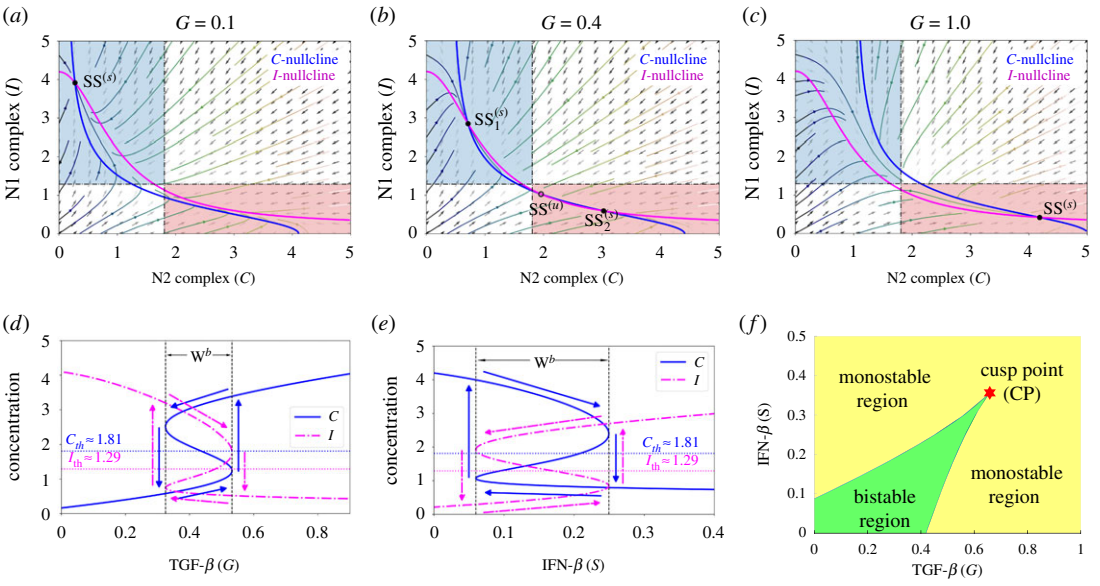

Figure 2. (*a–c*) Nullclines of model (2.1) in the *C*–*I* phase plane in response to (*a*) low, $G = 0.1$, (*b*) intermediate, $G = 0.4$, and (*c*) high, $G = 1$ levels of TGF-β showing the corresponding steady states where $SS^{(s)}$ and $SS^{(u)}$ denote stable, respectively, unstable steady state. Anti-tumorigenic and tumorigenic regions are marked in blue and pink boxes in (*a–c*). (*d*,*e*) Hysteresis diagram with respect to varying signals of TGF-β and IFN-β promoting N1-N2 on–off switch activation. (*f*) Codimension 2 bifurcation for different *G* and *S* levels depicting division of bistable and monostable region and a cusp point (CP).

unstable $SS^{(u)}$. Here, *S* represents the IFN-β-induced source of the N1 module. When TGF-β is low ($G = 0.1$), N2 complex activities are suppressed while N1 activities are promoted yielding one $SS^{(s)}$ which induces an anti-tumorigenic phenotype of TANs (figure 2*a*). On the contrary, high level of TGF-β ($G = 1.0$) enhances N2 activities but decreases that of N1 complex leading to a stable $SS^{(s)}$ which is a tumorigenic phenotype of TANs (figure 2*c*). Thus, for low and high *G* signals, phenotypic differentiation of TANs does not depend on initial status of N1 and N2 complexes. However, an intermediate TGF-β signal ($G = 0.4$) leads to two $SS^{(s)}$ and one $SS^{(u)}$ generating bistability in the system. The initial conditions of N1 and N2 complex influence the induction of either anti- or pro-tumour TANs (figure 2*b*). Due to the dichotomous behaviour of TANs with respect to signals of TGF-β, an associated hysteresis diagram is expected (figure 2*d*). The bistability window $W^b \approx [0.33, 0.53]$ provides the limit points for which the system jumps from one stable state to the other. The system is not only *G*-dependent but also *S*-dependent. That is, varying levels of IFN-β signals also promotes bistability and hysteresis as shown in figure 2*e*, where the bistability window with respect to *S* is $W^b \approx [0.06, 0.25]$. Note that the domain of bistability is dependent on key parameters and may progressively shrink for some parameter sets. Figure 2*f* depicts the bistable and monostable region under varying *G* and *S* simultaneously. Starting at a limit point obtained from one-parameter bifurcation (*G*), a cusp point (CP) is achieved by computing a fold continuation. Then, two key parameters *G* and *S* are increased (or decreased) at the same time along the trajectory of a limit point for equilibrium curve at the corresponding value of *S*. This resulted to a codim 2 bifurcation. The cusp point yields the threshold values C_{th} and I_{th}. `MatCont` was used for numerical continuation and bifurcation analysis [71]. In this study, the effects of exogenous intervention of TGF-β inhibitor and IFN-β on tumour progression are further investigated. Figure 1*a* illustrates the response of N1 and N2 complexes to the TGF-β inhibitor and IFN-β, acting as *regulatory controls* to the system. Note that N2-polarization by TGF-β can be blocked by using inhibitor (TGF-β Inh) and/or IFN-β promoting N1-dominant microenvironment. As depicted, both controls could downregulate N2 complex which activates N1 complex leading to tumour-suppression. Note that IL-6 is a protein-coding gene that induces Treg and others (upward arrow), which promotes N2 phenotype resulting in tumour growth. The dashed arrow indicates that withdrawal of IL-6 activity downregulates Treg and others (hence, downward arrow), leading to N1 phenotype suppressing tumours. Figure 1*b* shows the schematic diagram of the simplified model while figure 1*c* is the dimensionless form; N1 and N2 complexes are grouped as module *C* and *I*, respectively.

The non-dimensional set of differential equations describing the model is as follows:

$$\left.\begin{aligned}
\frac{\mathrm{d}L}{\mathrm{d}t} &= u_{\mathrm{L}}(t) - \mu_{\mathrm{L}}L,\\
\frac{\mathrm{d}G}{\mathrm{d}t} &= G_{\mathrm{S}} - \mu_{\mathrm{G}}G - \gamma_{\mathrm{L}}LG,\\
\frac{\mathrm{d}C}{\mathrm{d}t} &= \lambda + \lambda_{\mathrm{G}}G + \frac{k_1}{k_3^2 + \alpha I^2} - C,\\
\frac{\mathrm{d}S}{\mathrm{d}t} &= u_{\mathrm{S}}(t) - \mu_{\mathrm{S}}S,\\
\frac{\mathrm{d}I}{\mathrm{d}t} &= \lambda_{\mathrm{S}}S + \frac{k_2}{k_4^2 + \beta C^2} - \mu I\\
\text{and}\quad \frac{\mathrm{d}T}{\mathrm{d}t} &= r\left(1 + \frac{C}{K + \gamma_1 I}\right)T\left(1 - \frac{T}{T_0}\right) - \delta IT,
\end{aligned}\right\} \tag{2.2}$$

where u_{L} and u_{S} denote the exogenous infusion rate of TGF-β inhibitor and IFN-β, respectively, and T is the tumour volume.

The current modelling approach uses *optimal control theory* to identify therapeutic infusion protocol of TGF-β inhibitor and IFN-β that could lead to N1-polarization suppressing tumour progression. In particular, we aim to determine appropriate drug injection rates $u_{\mathrm{L}}(t)$ and/or $u_{\mathrm{S}}(t)$ minimizing tumour volume and associated administrative infusion cost. The controls u_{L} and u_{S} represent dosages of TGF-β inhibitor and an IFN-β drug, respectively. These controls are assumed to be bounded and Lebesgue integrable. That is, the control set is defined as

$$\Omega = \{(u_{\mathrm{L}}, u_{\mathrm{S}}) \big| u_i \quad \text{is measurable with } 0 \le u_i(t) \le u_i^{\max},\ t \in [t_0, t_1],\ i = L, S\}, \tag{2.3}$$

where $u_L^{\max}$ and $u_S^{\max}$ are the maximum tolerated TGF-β inhibitor and an IFN-β drug doses, respectively, which could be administered in a given treatment period. These upper bounds may also be viewed as the maximum amounts a patient can financially afford. The lower bounds for u_{L} and u_{S} correspond to no treatment. Furthermore, we intend to administer precisely the amount of treatment to be given to the patient over the given time interval $[t_0, t_1]$, which is within safety limits (*isoperimetric constraint*). That is, we have

$$\int_{t_0}^{t_1} u_{\mathrm{L}}(t)\,\mathrm{d}t = A_1 \quad \text{and} \quad \int_{t_0}^{t_1} u_{\mathrm{S}}(t)\,\mathrm{d}t = A_2, \tag{2.4}$$

where A_1 and A_2 are the known TGF-β inhibitor and IFN-β drug amounts, respectively. Considering the bounds for u_{L} and u_{S}, the choices for A_1 and A_2 satisfy

$$0 \le A_1 \le u_L^{\max}(t_1 - t_0) \quad \text{and} \quad 0 \le A_2 \le u_S^{\max}(t_1 - t_0).$$

The following optimal control problems (OCPs) are formulated to examine different therapeutic strategies. Here, the control costs are modelled by linear combination of quadratic terms, where the weight factors B_1 and B_2 denote the relative cost of minimizing tumour volume $T(t)$ and administering TGF-β inhibitor and/or IFN-β drug infusions over a certain time period, respectively. The quadratic form of the cost functional with respect to the controls ensures that the associated Hamiltonian becomes strictly convex and has a unique minimizer, thus making the mathematical problem more tractable. The use of such quadratic functionals is not commonly motivated by biological phenomena making its simplifying assumptions questionable [72]. However, its use in order to incorporate the nonlinearity of the problem has produced qualitatively significant results [73,74]. It should be noted that the quadratic controls in the cost function model the adverse effects of using too much drugs, as used in several works [73,75–79]. An isoperimetric optimal control has been applied to cancer immunotherapy [80–82].

1. *TGF-β inhibitor control only*. In this scheme, we want to investigate the anti-tumour effect of TGF-β inhibitor on tumour growth. In particular, we want to minimize the tumour size (T) and dose of TGF-β inhibitor while keeping the same IFN-β supply. Thus, the OCP is to minimize the cost

functional

$$J(u_{\mathrm{L}}(t)) = \int_{t_0}^{t_1} \left(T(t) + \frac{B_1}{2} u_{\mathrm{L}}^2(t) \right) \mathrm{d}t, \tag{2.5}$$

subject to (2.2) where S is assumed constant (i.e. $S = 0.2$, $\mathrm{d}S/\mathrm{d}t = 0$) with $\int_{t_0}^{t_1} u_{\mathrm{L}}(t)\,\mathrm{d}t = A_1$.

2. *IFN-β control only*. We consider the anti-tumour efficacy of IFN-β infusion. In particular, we want to minimize the tumour size (T) and dose of IFN-β in the absence of IFN-β inhibitor. Thus, the problem is formulated as minimizing the cost functional

$$J(u_{\mathrm{S}}(t)) = \int_{t_0}^{t_1} \left(T(t) + \frac{B_2}{2} u_{\mathrm{S}}^2(t) \right) \mathrm{d}t, \tag{2.6}$$

subject to (2.2) with constant TGF-β and no inhibitor present (i.e. $G = 0.45$, $\mathrm{d}G/\mathrm{d}t = 0$, $L = 0$, $\mathrm{d}L/\mathrm{d}t = 0$) with $\int_{t_0}^{t_1} u_{\mathrm{S}}(t)\,dt = A_2$.

3. *Concomitant TGF-β inhibitor and IFN-β controls*. In this approach, the anti-tumour efficacy of both controls is examined assuming that TGF-β inhibitor and IFN-β can be administered simultaneously. Specifically, we want to minimize the tumour size (T) and doses of both TGF-β inhibitor and IFN-β. Hence, the OCP is to minimize

$$J(u_{\mathrm{L}}(t), u_{\mathrm{S}}(t)) = \int_{t_0}^{t_1} \left(T(t) + \frac{B_1}{2} u_{\mathrm{L}}^2(t) + \frac{B_2}{2} u_{\mathrm{S}}^2(t) \right) \mathrm{d}t, \tag{2.7}$$

subject to (2.2) and isoperimetric constraints (2.4).

4. *Alternating TGF-β inhibitor and IFN-*β *controls*. In order to avoid drug complications such as risk of killing healthy cells and overdose, we propose a strategy of administering drugs alternately. Specifically, we want to minimize the tumour size (T) and doses of both TGF-β inhibitor and IFN-β in an alternating injection scheme. Thus, the OCP can then be formulated as minimizing the cost functional

$$\begin{aligned} J(u_{\mathrm{L}}(t), u_{\mathrm{S}}(t)) = &\int_{t_0}^{t_1} \left(T(t) + \frac{B_1}{2} u_{\mathrm{L}}^2(t) \right) \mathrm{d}t \\ &+ \int_{t_0'}^{t_1'} \left(T(t) + \frac{B_2}{2} u_{\mathrm{S}}^2(t) \right) \mathrm{d}t \end{aligned} \tag{2.8}$$

subject to (2.2) and isoperimetric constraints (2.4) within an appropriate time interval.

Our goal is to find optimal infusion regimen for TGF-β inhibitor and/or IFN-β, $\mathbf{u}^*(t) = (u_{\mathrm{L}}^*(t), u_{\mathrm{S}}^*(t))$ such that

$$J(\mathbf{u}^*(t)) = \min_{\Omega} J(\mathbf{u}(t)), \tag{2.9}$$

where Ω is the set of all square integrable functions $u_{\mathrm{L}}(t)$ and $u_{\mathrm{S}}(t)$ over a specified interval given in (2.3). By using standard results in control theory, the existence of optimal controls is guaranteed [83]. In this optimal control problem (OCP), the integrand of the objective functional satisfies the necessary convexity, in which Pontryagin's maximum principle can be applied [84]. In solving the OCP, an iterative method is used where initial conditions for the state variables and terminal conditions for the adjoints constitute a two-point boundary value problem. State equations are solved forward in time using the given initial conditions and the corresponding adjoint equations are solved backward in time starting with the transversality conditions. This is known as the forward–backward sweep method (FBSM). Numerical simulations can be obtained using Euler scheme or fourth-order iterative Runge–Kutta method. We use adapted FBSM [85,86] with adapted scheme [87] for isoperimetric constraints.

3. Results and discussion

In this section, we present the numerical results obtained from different control strategies. The weight parameters $B_1 = B_2 = 1$ are used as default values. Four different initial conditions, $Q_i := (C_{0,i}, I_{0,i})$, $i = 1, \ldots, 4$, are considered in order to resemble diverse phenotypical state of N1 and N2 complexes. The polarization of the microenvironment is N2-dominant if $C > C_{\mathrm{th}}$ and $I < I_{\mathrm{th}}$, otherwise, N1-dominant when $C < C_{\mathrm{th}}$ and $I > I_{\mathrm{th}}$. We include the following conditions:

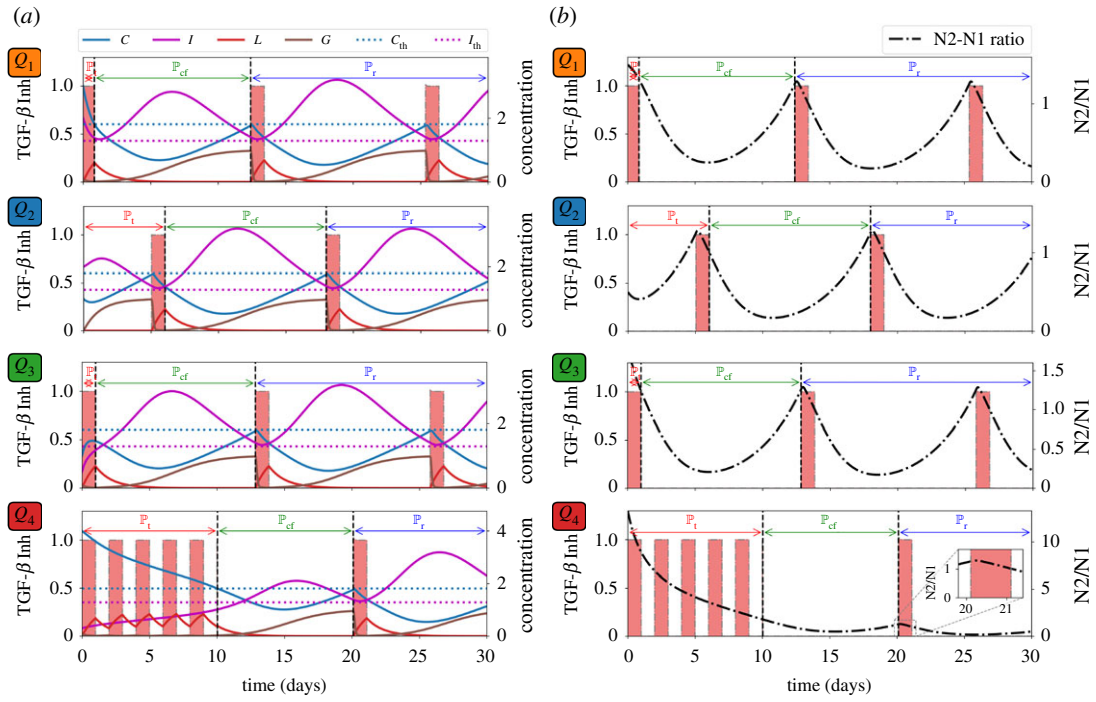

Figure 3. TGF-β inhibitor administration schedule under different initial conditions Q_1, Q_2, Q_3, Q_4 and corresponding dynamics of (*a*) C, I, L, G, and (*b*) N2/N1 levels. Administration of TGF-β inhibitor decreases the N2/N1 levels.

— $Q_1 = (3, 2)$: low-risk state, high levels of both C and I above their corresponding threshold values;
— $Q_2 = (1, 2)$: risk-free state, low (high) level of C (I) below (above) the threshold value;
— $Q_3 = (1, 0.5)$: low-risk state, low levels of C and I below their corresponding threshold values; and
— $Q_4 = (4, 0.3)$: high-risk state, high (low) level of C (I) above (below) the threshold value.

An important phenotypic marker is

$$C < C_{th} \quad \text{and} \quad I > I_{th}. \tag{3.1}$$

3.1. TGF-β inhibitor control only

In this therapeutic strategy, we assume that there is a constant source of IFN-β and that the system can be regulated by exogenously administering TGF-β inhibitor. The goal is to obtain optimal infusion protocol with the least cost of TGF-β inhibitor infusion, i.e. $u_L^*(t)$ that represses the N2-dominant phenotype leading to tumour-suppression. We consider that the total dose of TGF-β inhibitor which can be administered in a day is 1 unit, and thus, $A_1 = 1$. Also, we presume that this drug can only be administered every other day as in experiments [37] taking into account its toxicity to healthy tissue. The adapted FBSM is applied for (a maximum of) one day if condition (3.1) is not satisfied (i.e. either $C > C_{th}$ or $I < I_{th}$ or both inequalities hold) to obtain the optimal control profile $u_L^*(t)$ for that period. It is expected that C will decrease since TGF-β inhibitor blocks the TGF-β promoting N2 phenotype which would in turn, upregulate N1 activities. Then, a day of no infusion follows letting the TGF-β inhibitor take effect. The activities of C and I are simultaneously monitored. At the time when condition (3.1) holds, infusion is stopped or no control is applied. Continuous monitoring of C and I profiles will be crucial in determining the next TGF-β inhibitor infusion. This routine suggests a TGF-β inhibitor control.

We consider the *treatment period* $\mathbb{P}_t$ to be the time when initial control infusion is administered until condition (3.1) fails. Then *cancer-free period* $\mathbb{P}_{cf}$ is shortly achieved when condition (3.1) is satisfied. Before C crosses C_{th} from below (I crosses I_{th} from above), optimal control is again applied proposing the specific time of TGF-β inhibitor administration, and that commences the *relapse period* $\mathbb{P}_r$. Figure 3*a* depicts the control scheme, the corresponding profile of TGF-β inhibitor (L) and its effect on TGF-β (G), and the concentration profiles of C and I with different initial conditions Q_1, Q_2, Q_3, Q_4. For instance, if one considers Q_4 as initial values of C and I, TGF-β inhibitor control is applied every other

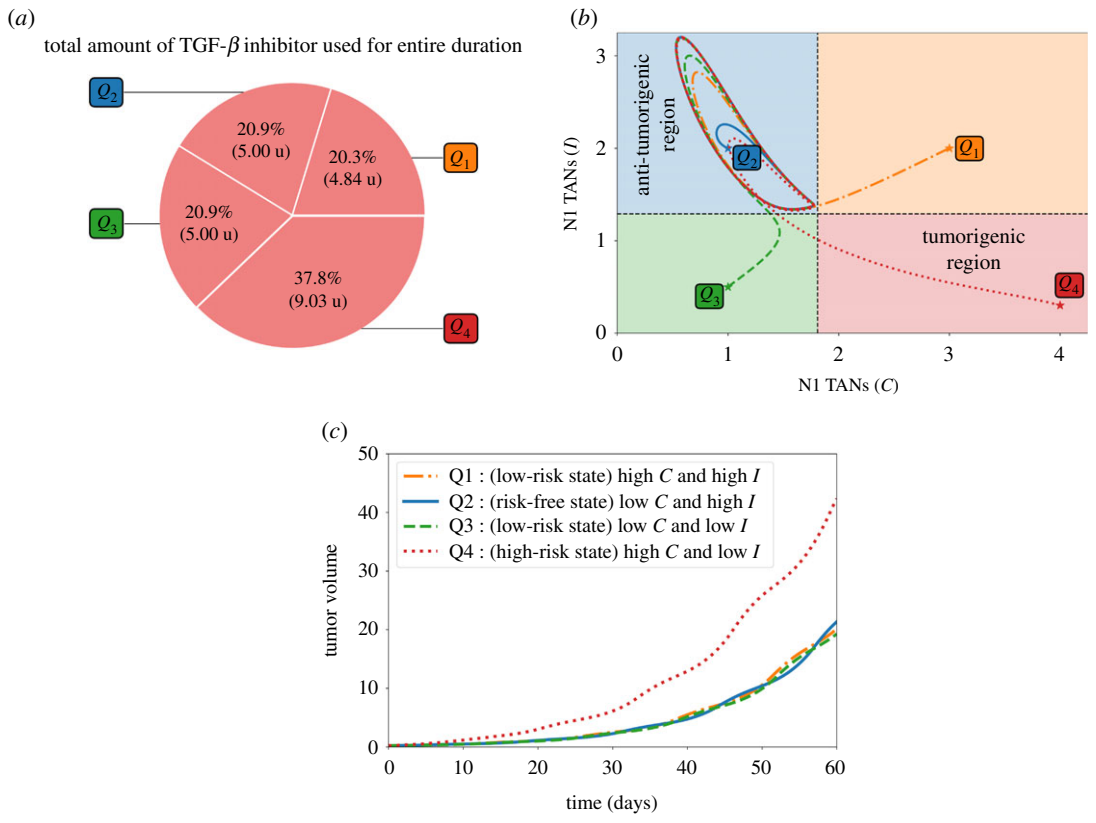

Figure 4. (*a*) Proportion of the amount of TGF-β inhibitor used for the entire treatment duration, (*b*) dynamics of the N1-N2 system and (*c*) tumour dynamics under TGF-β inhibitor control starting at different initial conditions Q_1, Q_2, Q_3, Q_4.

day until C crosses C_{th} which is about 10 days, duration of $\mathbb{P}_t$. Then $\mathbb{P}_{cf}$ follows until around day 20 when TGF-β inhibitor administration is again needed. The remaining time period covers $\mathbb{P}_r$. Note also that starting at risk-free, anti-tumorigenic region Q_2 satisfies condition (3.1). Thus, initial TGF-β inhibitor infusion commences (later) at around day 5. Figure 3*b* illustrates that administration of TGF-β inhibitor is needed to reduce the N2/N1 ratio (shown in black, dash-dotted curve). It is expected that when the initial condition is at high-risk, tumorigenic region Q_4, the total amount of TGF-β inhibitor to be used for entire medication period (60 days) is the largest. This is shown in figure 4*a*. The C–I dynamics obtained from the TGF-β inhibitor control protocol at different initial conditions are illustrated in figure 4*b*. Observe that all the trajectories converge to the anti-tumorigenic region. Time courses of tumour volume in these four cases illustrate the relatively poor anti-tumour efficacy when the initial condition is in the tumorigenic region Q_4 (figure 4*c*), despite the highest cost (figure 4*a*).

3.2. IFN-β control only

Let us consider a scenario when TGF-β inhibitor cannot be administered due to adverse drug reactions, high cost, etc., and assume that only IFN-β can be used for treatment purposes. Taking into account that IFN-β is a noxious drug [29,88,89], it can be administered only every other day in increasing amount as illustrated in experimental system [29,33,44]. In this strategy, we let the minimum and maximum IFN-β amount be 2 and 10 units, respectively (i.e. $A_2^{\min} = 2$, $A_2^{\max} = 10$). As in the first control strategy, both C and I are assessed. If condition (3.1) fails, then immediate administration of IFN-β is needed. This is done by using adapted FBSM for a day to fully utilize the minimum amount followed by a period of no infusion (maximum of a day) where both C and I are concurrently monitored. If condition (3.1) still does not hold, application of control routine is carried out where IFN-β amount is increased by 2 units. This infusion scheme with increasing amount of IFN-β per administration is implemented until condition (3.1) is not satisfied. The period from first IFN-β control administration until the last infusion where at least one of the inequalities in condition (3.1) no longer holds is what we refer to as the *treatment period* $\mathbb{P}_t$. Then a *critical period* $\mathbb{P}_{crit}$ follows where both C and I should be carefully

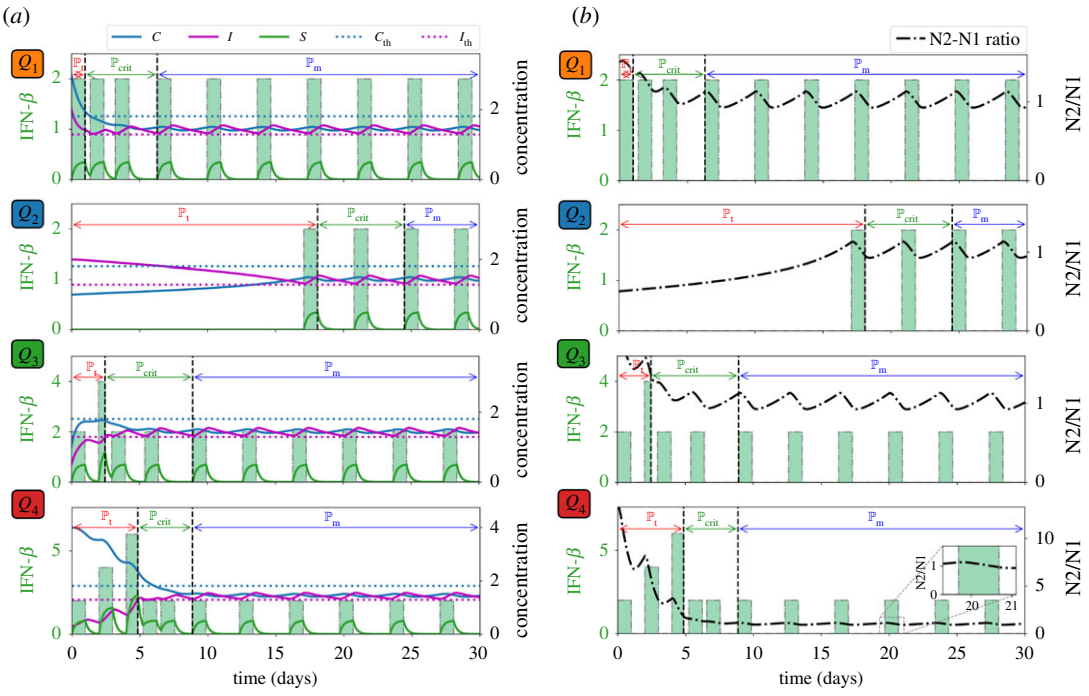

Figure 5. IFN-β administration schedule under different initial conditions Q_1, Q_2, Q_3, Q_4 and corresponding dynamics of (*a*) *C*, *I*, *S* and (*b*) N2/N1 levels. Administration of IFN-β lowers the N2/N1 levels.

monitored and strategic IFN-β infusion is necessary. Subsequently, *C* and *I* levels will be below and above their threshold values and IFN-β can be regularly administered at minimum amount. This period is considered as the *maintenance period* $\mathbb{P}_m$.

Figure 5*a* illustrates the IFN-β infusion control scheme, the corresponding IFN-β concentration profiles, and dynamics of *C* and *I*. It is shown that starting at Q_4 entails an increasing rate and amount of IFN-β infusion, and longer $\mathbb{P}_t$. It is interesting to note that with initial condition at Q_3, the second infusion rate during $\mathbb{P}_t$ is 2 units but it can be verified that the amount of IFN-$\beta < 2$. It can be observed in figure 5*b* that IFN-β infusion decreases the N2/N1 ratio levels.

It is depicted in figure 6*a* that the total amount of IFN-β needed for the entire medication duration for 60 days is the least when (*C*, *I*) is initially at anti-tumorigenic region Q_2 as opposed to starting at tumorigenic region Q_4. In figure 6*b*, the dynamics of *C*–*I* with different initial conditions under the IFN-β control are steered towards the anti-tumorigenic region. Relatively efficient treatment results starting from anti-tumorigenic sector Q_2 and poor outcomes starting from tumorigenic status Q_4 are reflected in time courses of tumour volumes in figure 6*c*.

3.3. Concomitant TGF-β inhibitor and IFN-β controls

Now let us assume that both TGF-β inhibitor and IFN-β can be administered concurrently. As in the previous strategies, drug infusions can be done every other day where IFN-β can be administered at an increasing amount. Both drugs are concomitantly administered until condition (3.1) is satisfied which spans the treatment period $\mathbb{P}_t$. After the infusions, *C* and *I* will decrease and increase, respectively, for some time. Before *C* and *I* cross their corresponding threshold value from below and above, respectively, simultaneous drug administration should be carried out. This duration covers the cancer-free period $\mathbb{P}_{cf}$. Then continuous monitoring of *C* and *I* profiles are necessary to determine the time for next concomitant administrations of TGF-β inhibitor and IFN-β. These period is referred to as the relapse period $\mathbb{P}_r$. Concomitant infusion scheme, corresponding TGF-β inhibitor and IFN-β concentrations, and dynamics of the state variables starting at different initial conditions are depicted in figure 7*a*. The average levels of N2/N1 ratio for each regimen denoted by $\tau_{\mathbb{P}_t}$, $\tau_{\mathbb{P}_{cf}}$, $\tau_{\mathbb{P}_r}$ under various scenarios are depicted in figure 7*b*. Figure 8*a* shows a better comparison of the average amount of N1/N2 levels for each medication period under different conditions while figure 8*b* illustrates the ratio of the maximum (τ_{max}) and minimum (τ_{min}) N2/N1 levels for each condition. Obviously, τ_{max}/τ_{min} is highest at high-risk state Q_4.

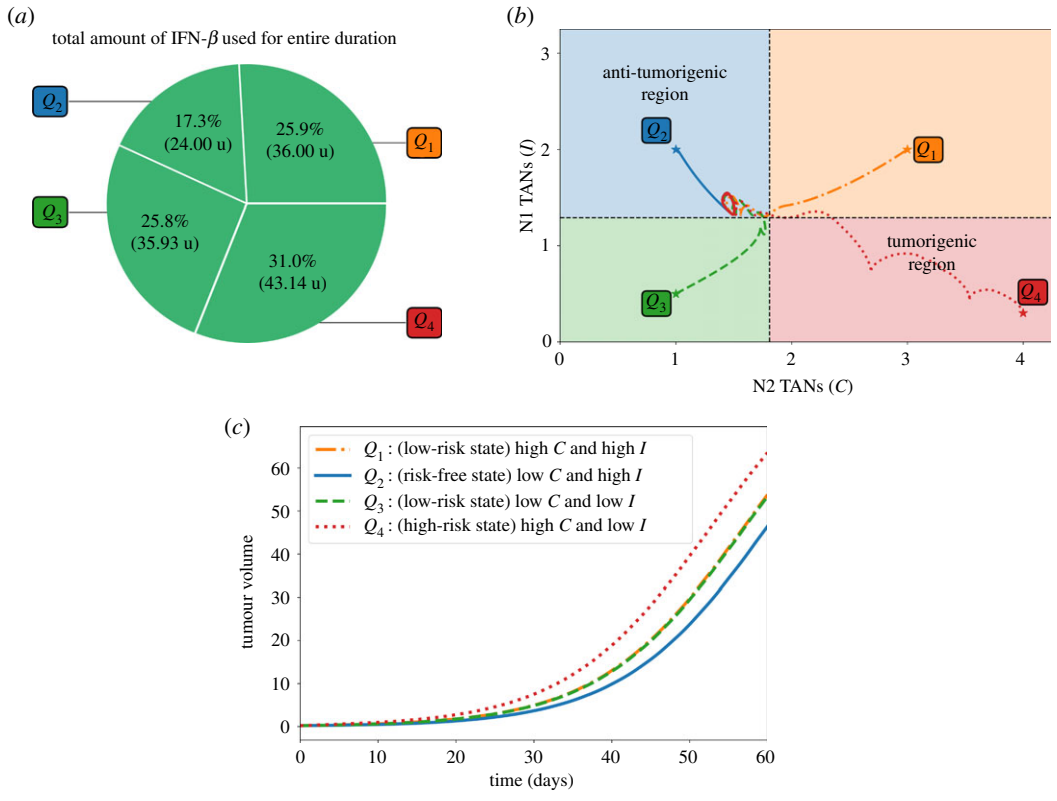

Figure 6. (*a*) Proportion of the amount of IFN-β used for the entire treatment duration, (*b*) dynamics of the N1-N2 system and (*c*) tumour dynamics under IFN-β control starting at different initial conditions Q_1, Q_2, Q_3, Q_4.

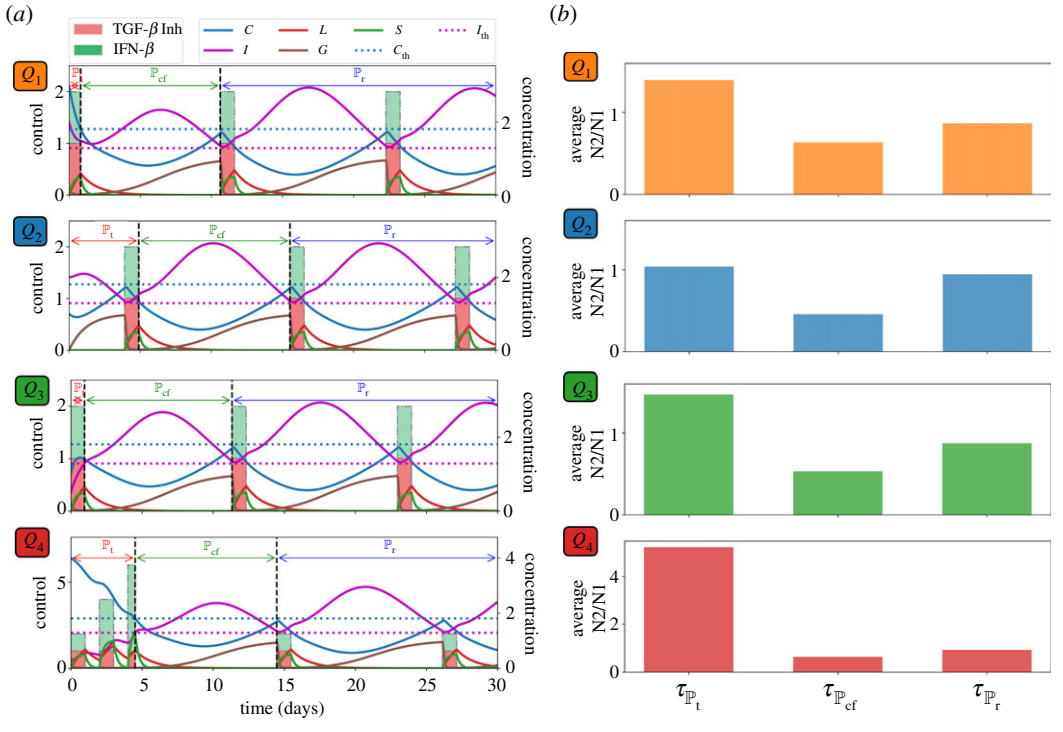

Figure 7. (*a*) Profiles of concomitant TGF-β inhibitor and IFN-β infusion protocol and corresponding concentration dynamics of *C*, *I*, *L*, *G*, *S*, and (*b*) average levels of N2/N1 (τ) for each period ($\mathbb{P}_t$, $\mathbb{P}_{cf}$, $\mathbb{P}_r$) starting at different initial conditions Q_1, Q_2, Q_3, Q_4.

The total amount of TGF-β inhibitor and IFN-β drugs administered for the entire medication duration of 60 days are depicted in figure 9*a*,*b*, respectively. It can be observed that starting at Q_4 needs more infusions and thus more drug amount used. On the contrary, less administration and drug amount is needed when (*C*, *I*) is initially at risk-free state Q_2. Figure 9*c* shows the *C*–*I* dynamics starting at different initial

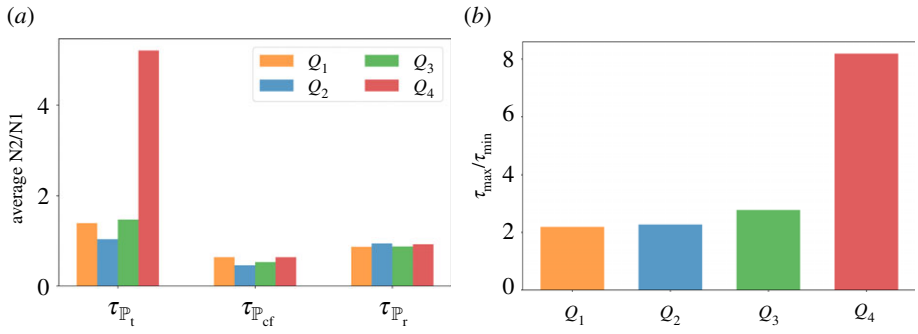

Figure 8. (*a*) Comparison of the average N2/N1 levels (τ) for each medication period ($\mathbb{P}_t$, $\mathbb{P}_{cf}$, $\mathbb{P}_r$) and (*b*) ratio of the maximum (τ_{max}) and minimum (τ_{min}) N2/N1 levels for each condition Q_1, Q_2, Q_3, Q_4 under concomitant TGF-β inhibitor and IFN-β scheme.

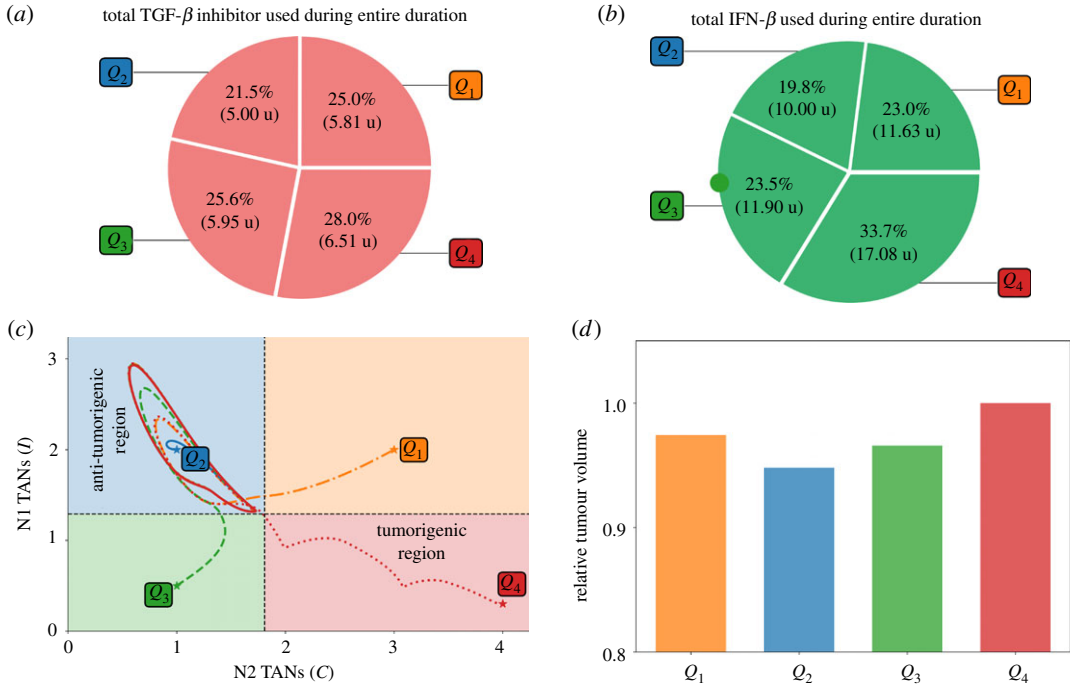

Figure 9. Proportion of the amount of TGF-β inhibitor (*a*) and IFN-β (*b*) used for the entire treatment duration, (*c*) dynamics of the N1-N2 system and (*d*) tumour volume relative to the high-risk state at the end simulation time under concomitant TGF-β inhibitor and IFN-β controls starting at different initial conditions Q_1, Q_2, Q_3, Q_4.

conditions. Administration of concomitant controls will drive all the trajectories to the anti-tumorigenic region. Scaled tumour volumes (Q_4 bar in figure 6*d*) and elongated path from the initial TAN distribution in the tumorigenic zone Q_4 (red dotted curve in figure 6*c*) also indicate the relatively worst outcome in decreasing the tumour size in the presence of a N2-dominant tumour microenvironment.

3.4. Alternating TGF-β inhibitor and IFN-β controls

Suppose that TGF-β inhibitor and IFN-β cannot be administered simultaneously due to toxicity, adverse drug reactions, etc. Here, we examine the scheme where drug infusion can be carried out alternately and every other day. Control scheme is obtained by analogously following the protocol and condition laid out in the previous strategies. The drug infusion protocol, its concentrations and state dynamics starting with different initial conditions are illustrated in figure 10*a* and the average levels of N2/N1 ratio $\tau_{\mathbb{P}_t}$, $\tau_{\mathbb{P}_{cf}}$, $\tau_{\mathbb{P}_r}$ under different conditions are illustrated in figure 10*b*. It is interesting to note that with initial condition at Q_1, IFN-β infusion is not necessary a day after the first TGF-β inhibitor administration. Also, starting at Q_3 needs lesser amount of IFN-β for its first infusion. Figure 11*a* shows a comparison of the average amount of N1/N2 levels for each medication period under different conditions while figure 11*b* illustrates the ratio of the maximum (τ_{max}) and minimum (τ_{min})

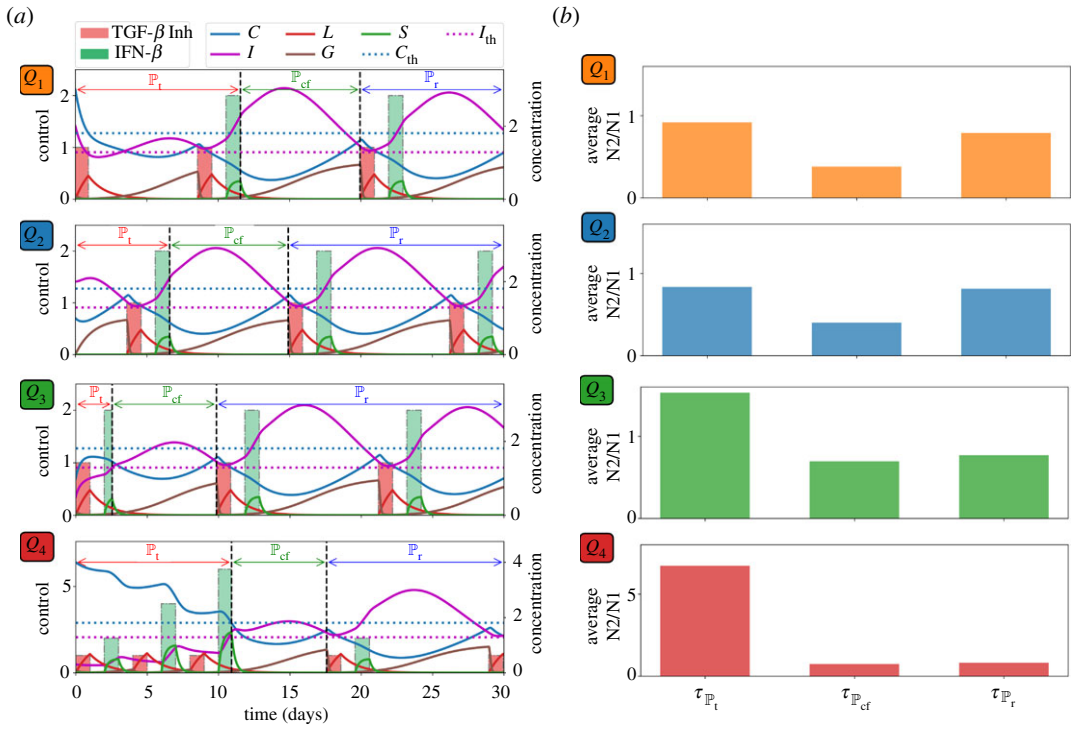

Figure 10. (*a*) Profiles of alternating TGF-β inhibitor and IFN-β infusion protocol and corresponding concentration dynamics of C, I, L, G, S, and (*b*) average levels of N2/N1 (τ) for each treatment period ($\mathbb{P}_t$, $\mathbb{P}_{cf}$, $\mathbb{P}_r$) starting at different initial conditions Q_1, Q_2, Q_3, Q_4.

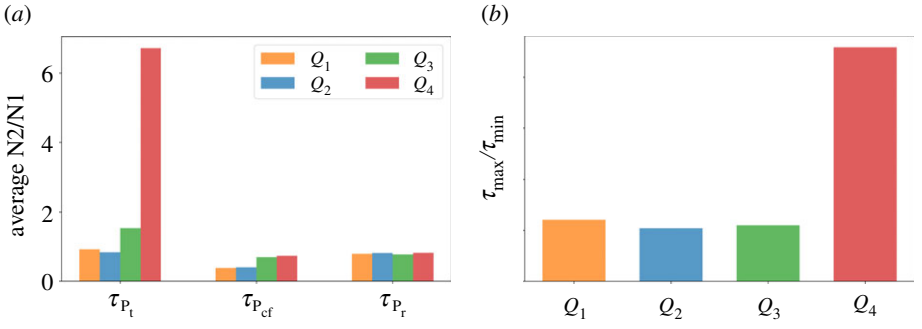

Figure 11. (*a*) Comparison of the average N2/N1 levels (τ) for each medication period ($\mathbb{P}_t$, $\mathbb{P}_{cf}$, $\mathbb{P}_r$) and (*b*) ratio of the maximum (τ_{max}) and minimum (τ_{min}) N2/N1 levels for each condition Q_1, Q_2, Q_3, Q_4 under alternating TGF-β inhibitor and IFN-β scheme.

N2/N1 levels for each condition under alternating administration of TGF-β inhibitor and IFN-β. As expected, τ_{max}/τ_{min} is highest at high-risk state Q_4.

The proportion and the total amount of TGF-β inhibitor and IFN-β used for the entire duration of 60 days are depicted in figure 12*a*,*b*, respectively. As expected, starting at Q_4 needs more drug infusions and hence more drug amount compared with other initial conditions. Trajectories of the C–I dynamics with different initial conditions towards the anti-tumorigenic region under the alternating control scheme are illustrated in figure 12*c*. Time courses of tumour volumes in four cases (figure 12*d*) show the worst outcome in decreasing the tumour size with the initial TAN distribution in the tumorigenic zone Q_4, indicating the critical role of the N1/N2 immune conditions. It is important to note that, in order to satisfy condition (3.1), the initial drug administration and infusion duration vary with different initial conditions. This in turn, influences the drug amount to be used within a specific period. Starting at Q_2, for instance, showed that drug infusion is not carried out during the first day. On the other hand, starting at Q_4 demands several drug administrations to meet the condition (3.1).

Figure 13 compares the relative total amount of TGF-β inhibitor and IFN-β used in the proposed therapeutic strategies starting at different initial conditions. Across the various schemes, starting at Q_4 needs a bigger amount to bring C below and keep I above their respective threshold values.

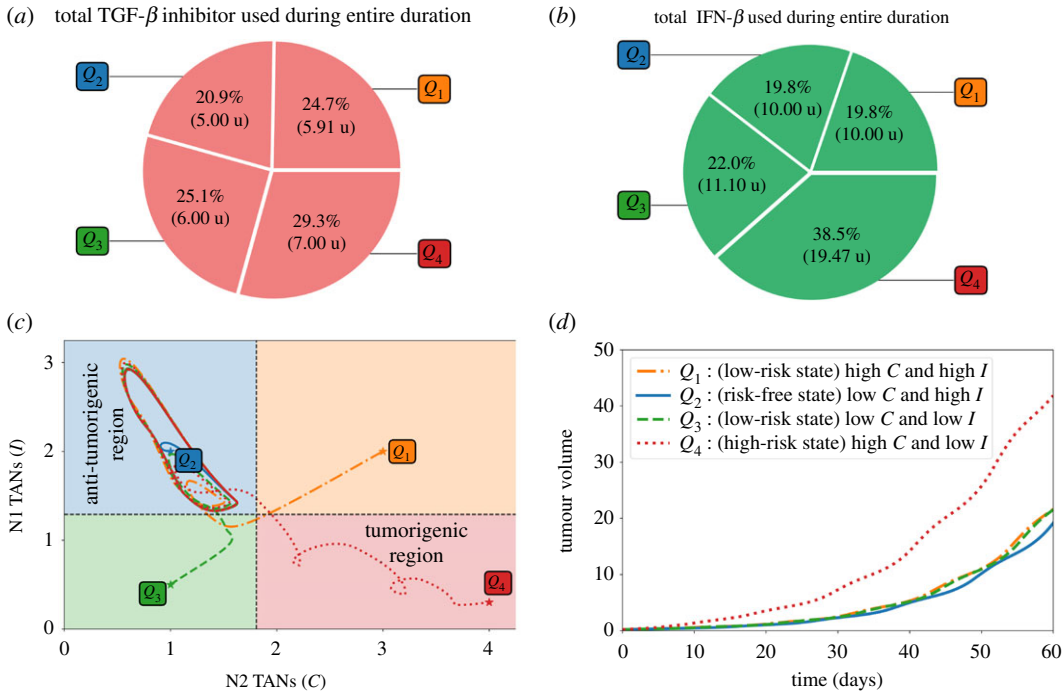

Figure 12. (*a*) Proportion of the amount of TGF-β inhibitor, (*b*) IFN-β used for the entire treatment duration, (*c*) dynamics of the N1-N2 system and (*d*) tumour dynamics under alternating TGF-β inhibitor and IFN-β controls starting at different initial conditions Q_1, Q_2, Q_3, Q_4.

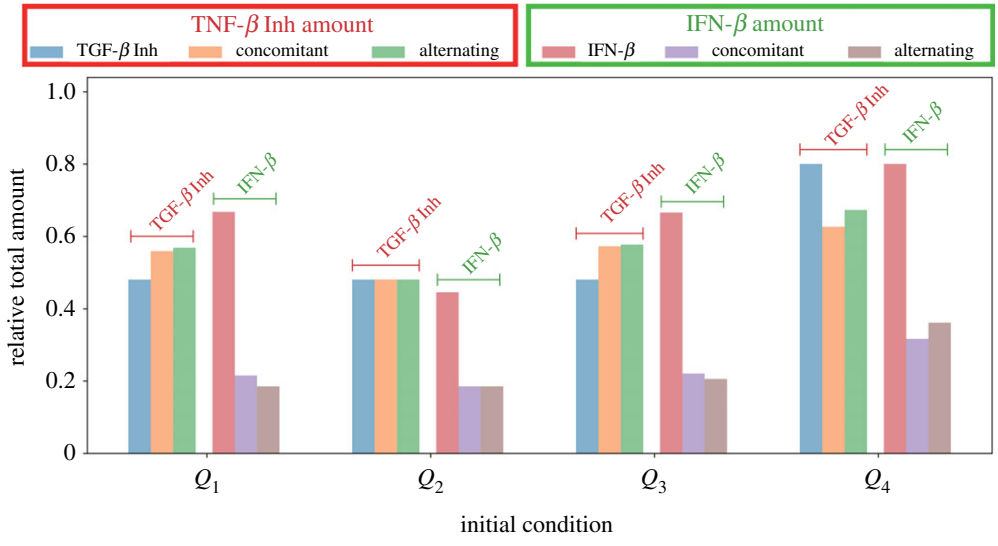

Figure 13. Relative amount of TGF-β inhibitor and IFN-β used among different control strategies.

4. Conclusion

The exact role of immune cells such as NK cells [4] and TANs in tumour growth is still poorly understood. Several studies have reported that neutrophils are cytotoxic to tumour cells. On the contrary, a growing clinical evidence supports that neutrophils can promote tumour progression by enhancing proliferation and angiogenesis, and inducing cell migration and metastasis [20,21,23]. Hence, TANs can display two different phenotypes: an anti-tumour (N1) and pro-tumour (N2) effector cells [15,16,24]. The current study investigates a regulatory model between N1 and N2 TANs. In this work, optimal control theory is employed to determine the amount, infusion times and cost of TGF-β inhibitor and IFN-β administrations to activate N1 leading to tumour suppression. This framework has been utilized to identify treatment schedules and anti-invasion therapy for

glioblastoma [90,91]. Both single and combination drug therapies are considered under various phenotypical conditions of N1 and N2. An important aspect of determining treatment protocol is the patients' pathophysiological condition. We identified therapeutic regimen for promoting anti-tumoural TANs and suppressing pro-tumoural neutrophil phenotypic states through four different administration of the TGF-β inhibitor and IFN-β in lung cancer. The optimal control scheme predicts that, depending on relative states of N1 and N2 phenotypes, therapy schedules may have to be adjusted properly to minimize adverse effects of these drugs and its administration cost in addition to maximizing anti-tumour efficacy.

Proper diagnosis of N1 and N2 activities are important tools in order to have an adaptive and individualized drug infusion protocol [60]. Converting N2 TANs to N1 could provide new therapeutic options for cancer treatment. Our work essentially can provide a general framework of *optimally controlled* injection schedules of anti-cancer drugs such as TGF-β inhibitors and IFN-β through immune control, i.e. a critical transition between N1 and N2 TANs. Immune cells in a tumour microenvironment play such a critical role in regulation of tumour growth and anti-cancer therapies [4], having two faces of anti-tumour and tumour-promoting roles. The mathematical framework in this work may be adapted for optimal results of anti-cancer therapies as far as appropriate patient-specific data in clinics are provided.

Our study has four limitations:

— The current work does not consider the role of other factors in TME such as intracellular pathways such as STAT1/STAT3/JAK [92] in response to IFN-β, TGF-β, and other stimuli [93], neutrophil elastase (NE) in the presence [94] and absence [95,96] of LPS, tumour-promoting or -suppressive immune response of NK cells [4,97], tumour-associated fibroblasts (TAFs) [67,98–100], ECM remodelling [69,101–103], angiogenesis from blood vessels [104–106], or growth factors such as EGF [107,108] and CSF-1 [5,109]. NK cells were shown to mediate dual roles of neutrophils in metastatic colonization [110,111]. For example, neutrophils can enhance extravasation of circulating tumour cells by suppressing NK cells [111]. Depletion or adjuvant therapy of NK cells was shown to increase anti-tumour efficacy in a combination therapy (OV-bortezomib-NK) relative to control, showing nonlinear behaviour of immune system [4]. These factors may play major roles in regulation of $N1 \rightarrow N2$ transition, thus cancer progression. In particular, we focused on the effect of TGF-β inhibitor and IFN-β on TANs in this study, but it would be important to see the effect of those two inhibitors on NK cells and TAFs in future work. For example, TGF-β and its inhibitor [98,99,112] and IFNs [112–115] play an important role in regulation of tumour-associated fibroblasts in cancer progression. We plan to include those players in a future optimal-control model.
— NET and NE were shown to promote tumour growth and invasion [116] by turning on the multiple signalling pathways including PI3K in lung cancer cells [117]. For example, upregulated NET activities near tumour sections induce the transformation of B cells [118], contributing to cancer progression [119]. In particular, mathematical models [116] and experimental data [120] suggest that NET can mediate the critical metastatic process [121,122] to stabilize the circulating tumour cells in the bloodstream and help extravasation of these cancerous cells. However, NET was also suggested to suppress tumour growth in colonic adenocarcinoma [123]. In our study, we did not take into account these critical influence of NETs in a spatial domain. We plan to develop an optimal control approach in a new framework of the partial differential equations of NETs in order to improve the therapeutic, anti-invasion strategies.
— Unforeseen microenvironmental factors may limit bi-lateral switches between N1 and N2 TANs. In our study, optimal control was applied only to IFN-β and TGF-β inhibitors. We plan to investigate the specific role and optimization of these stimuli in TME for better understanding of the role of TANs (either promotion [124–127] or suppression of tumour progression [123]). A new optimal control method has to be developed for a possible triple combination therapy, i.e. TGF-β + TGF-β inhibitor + immune agents [128]. We plan to develop an optimal control of the TAN's plasticity of the possibly continuous spectrum of the $N1 \rightarrow N2$ switches, which requires better understanding and experiments of the biological system as well as advanced optimal control theory.
— It has been reported that a more realistic clinical situation employs linear cost functions. These types of problems have been used in several works devoted to the administration of single and combination therapies to treat different types of tumours [129–133]. On the contrary, a study by Glick & Mastroberardino [74] concluded that quadratic control yields continuous, low doses of the therapeutic drug producing a better outcome in the eradication of the solid tumour. Several researches on optimal control approaches for cancer treatment still favour quadratic controls [77–79].

Under certain circumstances, both linear and quadratic controls obtain qualitatively similar results [76,81,134]. It is true that profiles of treatment strategies depend on the landscape of the cost functionals. These differences show the importance of carefully defining an objective functional that most accurately reflects the toxicities of a particular drug along with the objective of the treatment strategy, for instance, decreasing the tumour mass at the end of the treatment interval, reducing the overall tumour burden over the treatment interval, and some other clinically relevant criteria [73]. It is therefore suggested that further model iterations should include exhaustive investigations on linear controls to have holistic treatment strategies for cancer treatment. Further analysis of models with other types of objective functionals should also be pursued. Varying results should then be presented to the medical practitioner for them to decide which solutions best fit the biological situation and can be used for practical implementation, if any [134].

This work, however, provides a general framework of optimal control approach for the fundamental transition from N2 to N1 TANs, thus inhibiting tumour growth, in response to known key players.

Typical lifespan of neutrophils is usually under tight control for maintenance of tissue homeostasis due to their potential toxicity [135], leading to short half-life in blood circulation after leaving the bone marrow. However, there exist multiple cellular and molecular factors such as smoking and reactive oxygen species (ROS) [136–138] that can influence their longevity [139,140], altered signalling pathways and neutrophil apoptosis in TME [136,137,141,142]. For example, ROS production is shown to be decreased in the absence of endogenous IFN-β, inducing cellular delays in apoptosis of TANs [143]. Since these factors may affect a complex imbalance between N1 and N2 TANs, an optimal control framework of such N1/N2 system with *time delays* [144,145] is needed in order to control the aggressive promotion of aggressive tumour growth.

Building a mathematical model does not entail all important details of a life process, rather, distil key elements that could provide insight into the underlying mechanisms and generate novel hypotheses for experimentation [45]. Since no model is perfect, and is lacking some aspects of reality, a symbiotic approach incorporating *in vivo*, *in vitro* and *in silico* techniques could be proven to be beneficial [146,147]. Despite several caveats and limitations, mathematical modelling will still be instrumental in understanding cancer biology and treatment [47]. Further design of experiments and development of computational techniques for verification and validation should be carried out using experimental data. Various types of mathematical models were suggested for better understanding of tumour biology: (i) ordinary differential equations [60,91,148–152], (ii) delay differential equations [60,148,153], (iii) partial differential equations [4,5,67,68,101,103,116,154–160], (iv) immersed boundary method [161,162], (v) individual-based models [163–165], and (vi) multi-scale hybrid model [69,100,166–173]. See [174] for a review of cell-based approaches. These mathematical approaches have been applied to investigation of various aspects of signalling network of oncogenes and tumour suppressors, tumour growth, cellular invasion, angiogenesis, recurrence, interaction with tumour microenvironment including chemokines/cytokines, stromal cells, immune cells, metastasis and development of anti-cancer strategies. In particular, multi-scale mathematical models [69,100,166,167,169–173,175,176] could be used to address dynamical changes in inter- and intra-cellular signalling pathways at the microscale level and integrate cellular process at the cellular level. We hope to address these issues in future work.

Data accessibility. We deposited all codes and data within the Dryad Digital Repository: https://doi.org/10.5061/dryad.g79cnp5r0. We have two files: (1) README.txt (2) data_RSOS-210705.zip. Here, the zip file contains all codes and data.

Competing interests. The authors declare that they have no competing interests.

Funding. This work was supported by the National Research Foundation of Korea (NRF) grant funded by the Korea government (MSIT) (No. 2021R1A2C1010891) (Y.K.).

Acknowledgements. A.D.L.R.V. acknowledges the support of the Institute of Mathematics, University of the Philippines Diliman and the Institute for Basic Science (IBS-R029-C3).

References

1. Siegel RL, Miller KD, Jemal A. 2019 Cancer statistics, 2019. *CA Cancer J. Clin.* **69**, 7–34. (doi:10.3322/caac.21551)
2. Ferlay J, Colombet M, Soerjomataram I, Mathers C, Parkin DM, Piñeros M, Znaor A, Bray F. 2019 Estimating the global cancer incidence and mortality in 2018: GLOBOCAN sources and methods. *Int. J. Cancer* **144**, 1941–1953. (doi:10.1002/ijc.31937)
3. Jaillon S, Ponzetta A, Mitri DD, Santoni A, Bonecchi R, Mantovani A. 2020 Neutrophil diversity and plasticity in tumour progression and therapy. *Nat. Rev. Cancer* **20**, 485–503. (doi:10.1038/s41568-020-0281-y)
4. Kim Y, Yoo JY, Lee TJ, Liu J, Yu J, Caligiuri MA, Kaur B, Friedman A. 2018 Complex role of NK cells in regulation of oncolytic virus-bortezomib

therapy. *Proc. Natl Acad. Sci. USA* **115**, 4927–4932. (doi:10.1073/pnas.1715295115)
5. Kim Y, Jeon H, Othmer H. 2017 The role of the tumor microenvironment in glioblastoma: a mathematical model. *IEEE Trans. Biomed. Eng.* **64**, 519–527.
6. Choi EY, Santoso S, Chavakis T. 2009 Mechanisms of neutrophil transendothelial migration. *Front. Biosci. (Landmark edition)* **14**, 1596–1605. (doi:10.2741/3327)
7. Borregaard N. 2010 Neutrophils, from marrow to microbes. *Immunity* **33**, 657–670. (doi:10.1016/j.immuni.2010.11.011)
8. Voisin MB, Nourshargh S. 2013 Neutrophil transmigration: emergence of an adhesive cascade within venular walls. *J. Innate Immun.* **5**, 336–347. (doi:10.1159/000346659)
9. Bianchi ME. 2007 DAMPs, PAMPs and alarmins: all we need to know about danger. *J. Leukoc. Biol.* **81**, 1–5. (doi:10.1189/jlb.0306164)
10. Park SA, Hyun YM. 2016 Neutrophil extravasation cascade: what can we learn from two-photon intravital imaging? *Immune Netw.* **16**, 317–321. (doi:10.4110/in.2016.16.6.317)
11. Kolaczkowska E, Kubes P. 2013 Neutrophil recruitment and function in health and inflammation. *Nat. Rev. Immunol.* **13**, 159–175. (doi:10.1038/nri3399)
12. Pham CTN. 2006 Neutrophil serine proteases: specific regulators of inflammation. *Nat. Rev. Immunol.* **6**, 541–550. (doi:10.1038/nri1841)
13. Scapini P, Lapinet-Vera JA, Gasperini S, Calzetti F, Bazzoni F, Cassatella MA. 2000 The neutrophil as a cellular source of chemokines. *Immunol. Rev.* **177**, 195–203. (doi:10.1034/j.1600-065X.2000.17706.x)
14. Tecchio C, Scapini P, Pizzolo G, Cassatella MA. 2013 On the cytokines produced by human neutrophils in tumors. *Semin. Cancer Biol.* **23**, 159–170. The dichotomy of neutrophil granulocytes in cancer. (doi:10.1016/j.semcancer.2013.02.004)
15. Shaul ME *et al.* 2016 Tumor-associated neutrophils display a distinct N1 profile following TGFβ modulation: a transcriptomics analysis of pro- vs. antitumor TANs. *OncoImmunology* **5**, e1232221. (doi:10.1080/2162402X.2016.1232221)
16. Hagerling C, Werb Z. 2016 Neutrophils: critical components in experimental animal models of cancer. *Semin. Immunol.* **28**, 197–204. (doi:10.1016/j.smim.2016.02.003)
17. Sionov RV, Fridlender ZG, Granot Z. 2015 The multifaceted roles neutrophils play in the tumor microenvironment. *Cancer Microenviron.* **8**, 125–158. (doi:10.1007/s12307-014-0147-5)
18. Swierczak A, Mouchemore KA, Hamilton JA, Anderson RL. 2015 Neutrophils: important contributors to tumor progression and metastasis. *Cancer Metastasis Rev.* **34**, 735–751. (doi:10.1007/s10555-015-9594-9)
19. Liang W, Ferrara N. 2016 The complex role of neutrophils in tumor angiogenesis and metastasis. *Cancer Immunol. Res.* **4**, 83–91. (doi:10.1158/2326-6066.CIR-15-0313)
20. Schmidt H, Bastholt L, Geertsen P, Christensen IJ, Larsen S, Gehl J, Von Der Maase H. 2005 Elevated neutrophil and monocyte counts in peripheral blood are associated with poor survival in patients with metastatic melanoma: a prognostic model. *Br. J. Cancer* **93**, 273–278. (doi:10.1038/sj.bjc.6602702)
21. Bellocq A *et al.* 1998 Neutrophil alveolitis in bronchioloalveolar carcinoma: induction by tumor-derived interleukin-8 and relation to clinical outcome. *Am. J. Pathol.* **152**, 83–92.
22. Atzpodien J, Reitz M. 2008 Peripheral blood neutrophils as independent immunologic predictor of response and long-term survival upon immunotherapy in metastatic renal-cell carcinoma. *Cancer Biotherapy Radiopharm.* **23**, 129–134. (doi:10.1089/cbr.2007.0429)
23. Trellakis S *et al.* 2011 Polymorphonuclear granulocytes in human head and neck cancer: enhanced inflammatory activity, modulation by cancer cells and expansion in advanced disease. *Int. J. Cancer* **129**, 2183–2193. (doi:10.1002/ijc.25892)
24. Fridlender ZG, Sun J, Kim S, Kapoor V, Cheng G, Ling L, Worthen GS, Albelda SM. 2009 Polarization of tumor-associated neutrophil phenotype by TGF-β: 'N1' versus 'N2' TAN. *Cancer Cell* **16**, 183–194. (doi:10.1016/j.ccr.2009.06.017)
25. Saha S, Biswas S. 2016 Tumor-associated neutrophils show phenotypic and functional divergence in human lung cancer. *Cancer Cell* **30**, 11–13. (doi:10.1016/j.ccell.2016.06.016)
26. Shen L, Smith JM, Shen Z, Eriksson M, Sentman C, Wira CR. 2007 Inhibition of human neutrophil degranulation by transforming growth factor-beta1. *Clin. Exp. Immunol.* **149**, 155–161. (doi:10.1111/j.1365-2249.2007.03376.x)
27. Andzinski L *et al.* 2016 Type I IFNs induce anti-tumor polarization of tumor associated neutrophils in mice and human. *Int. J. Cancer* **138**, 1982–1993. (doi:10.1002/ijc.29945)
28. Jablonska J, Leschner S, Westphal K, Lienenklaus S, Weiss S. 2010 Neutrophils responsive to endogenous IFN-β regulate tumor angiogenesis and growth in a mouse tumor model. *J. Clin. Invest.* **120**, 1151–1164. (doi:10.1172/JCI37223)
29. Studeny M, Marini FC, Dembinski JL, Zompetta C, Cabreira-Hansen M, Bekele BN, Champlin RE, Andreeff M. 2004 Mesenchymal stem cells: potential precursors for tumor stroma and targeted-delivery vehicles for anticancer agents. *JNCI: J. Natl Cancer Inst.* **96**, 1593–1603. (doi:10.1093/jnci/djh299)
30. Takaoka A *et al.* 2003 Integration of interferon-α/β signalling to p53 responses in tumour suppression and antiviral defence. *Nature* **424**, 516–523. (doi:10.1038/nature01850)
31. Zhang F, Sriram S. 2009 Identification and characterization of the interferon-β-mediated p53 signal pathway in human peripheral blood mononuclear cells. *Immunology* **128**, e905–e918. (doi:10.1111/j.1365-2567.2009.03104.x)
32. Garcia-Diaz A *et al.* 2017 Interferon receptor signaling pathways regulating PD-L1 and PD-L2 expression. *Cell Rep.* **19**, 1189–1201. (doi:10.1016/j.celrep.2017.04.031)
33. Catani JPP *et al.* 2016 Intratumoral immunization by p19Arf and interferon-β gene transfer in a heterotopic mouse model of lung carcinoma. *Transl. Oncol.* **9**, 565–574. (doi:10.1016/j.tranon.2016.09.011)
34. Chiantore MV *et al.* 2012 Interferon-β induces cellular senescence in cutaneous human papilloma virus-transformed human keratinocytes by affecting p53 transactivating activity. *PLoS ONE* **7**, e36909. (doi:10.1371/journal.pone.0036909)
35. Takaoka A *et al.* 2003 Integration of interferon-alpha/beta signalling to p53 responses in tumour suppression and antiviral defence. *Nature* **424**, 516–523. (doi:10.1038/nature01850)
36. Herbertz S *et al.* 2015 Clinical development of galunisertib (LY2157299 monohydrate), a small molecule inhibitor of transforming growth factor-beta signaling pathway. *Drug Design, Dev. Therapy* **9**, 4479–4499. (doi:10.2147/DDDT.S86621)
37. Holmgaard RB *et al.* 2018 Targeting the TGFβ pathway with galunisertib, a TGFβRI small molecule inhibitor, promotes anti-tumor immunity leading to durable, complete responses, as monotherapy and in combination with checkpoint blockade. *J. Immunother Cancer* **6**, 47. (doi:10.1186/s40425-018-0356-4)
38. Yingling JM *et al.* 2017 Preclinical assessment of galunisertib (LY2157299 monohydrate), a first-in-class transforming growth factor-β receptor type I inhibitor. *Oncotarget* **9**, 6659–6677. (doi:10.18632/oncotarget.23795)
39. Serova M *et al.* 2015 Effects of TGF-beta signalling inhibition with galunisertib (LY2157299) in hepatocellular carcinoma models and in ex vivo whole tumor tissue samples from patients. *Oncotarget* **6**, 21 614–21 627. (doi:10.18632/oncotarget.4308)
40. Wick A *et al.* 2020 Phase 1b/2a study of galunisertib, a small molecule inhibitor of transforming growth factor-beta receptor I, in combination with standard temozolomide-based radiochemotherapy in patients with newly diagnosed malignant glioma. *Invest. New Drugs* **38**, 1570–1579. (doi:10.1007/s10637-020-00910-9)
41. He X, Guo X, Zhang H, Kong X, Yang F, Zheng C. 2017 Mechanism of action and efficacy of LY2109761, a TGF-β receptor inhibitor, targeting tumor microenvironment in liver cancer after TACE. *Oncotarget* **9**, 1130–1142. (doi:10.18632/oncotarget.23193)
42. Melisi D, Ishiyama S, Sclabas GM, Fleming JB, Xia Q, Tortora G, Abbruzzese JL, Chiao PJ. 2008 LY2109761, a novel transforming growth factor β receptor type I and type II dual inhibitor, as a therapeutic approach to suppressing pancreatic cancer metastasis. *Mol. Cancer Ther.* **7**, 829–840. (doi:10.1158/1535-7163.MCT-07-0337)
43. Ghosh D, Parida P. 2016 Interferon therapy in lung cancer: current perspectives. *Curr. Cancer Therapy Rev.* **12**, 237–245. (doi:10.2174/1573394713666170316124158)
44. Patel MR *et al.* 2015 Vesicular stomatitis virus expressing interferon-β is oncolytic and promotes antitumor immune responses in a syngeneic murine model of non-small cell lung cancer. *Oncotarget* **6**, 33 165–33 177. (doi:10.18632/oncotarget.5320)
45. Anderson ARA, Quaranta V. 2008 Integrative mathematical oncology. *Nat. Rev. Cancer* **8**, 227–234. (doi:10.1038/nrc2329)
46. Byrne HM. 2010 Dissecting cancer through mathematics: from the cell to the animal

model. *Nat. Rev. Cancer* **10**, 221–230. (doi:10.1038/nrc2808)
47. Altrock PM, Liu LL, Michor F. 2015 The mathematics of cancer: integrating quantitative models. *Nat. Rev. Cancer* **15**, 730–745. (doi:10.1038/nrc4029)
48. Hoffmann K *et al.* 2020 Integration of mathematical model predictions into routine workflows to support clinical decision making in haematology. *BMC Med. Inform. Decis. Mak.* **20**, 28. (doi:10.1186/s12911-020-1039-x)
49. Fors J, Strydom N, Fox WS, Keizer RJ, Savic RM. 2020 Mathematical model and tool to explore shorter multi-drug therapy options for active pulmonary tuberculosis. *PLoS Comput. Biol.* **16**, e1008107. (doi:10.1371/journal.pcbi.1008107)
50. Hamis S, Powathil GG, Chaplain MAJ. 2020 Blackboard to bedside: a mathematical modeling bottom-up approach toward personalized cancer treatments. *JCO Clin. Cancer Inform.* **3**, 1–11. (doi:10.1200/CCI.18.00068)
51. Agur Z, Vuk-Pavlović S. 2012 Mathematical modeling in immunotherapy of cancer: personalizing clinical trials. *Mol. Ther.* **20**, 1–2. (doi:10.1038/mt.2011.272)
52. Eletreby R, Zhuang Y, Carley KM, Yagan O, Poor HV. 2020 The effects of evolutionary adaptations on spreading processes in complex networks. *Proc. Natl Acad. Sci. USA* **117**, 5664–5670. (doi:10.1073/pnas.1918529117)
53. Bekisz S, Geris L. 2020 Cancer modeling: from mechanistic to data-driven approaches, and from fundamental insights to clinical applications. *J. Comput. Sci.* **46**, 101198. (doi:10.1016/j.jocs.2020.101198)
54. Bozic I *et al.* 2013 Evolutionary dynamics of cancer in response to targeted combination therapy. *eLife* **2**, e00747. (doi:10.7554/eLife.00747)
55. Komarova NL, Wodarz D. 2005 Drug resistance in cancer: principles of emergence and prevention. *Proc. Natl Acad. Sci. USA* **102**, 9714–9719. (doi:10.1073/pnas.0501870102)
56. Leder K, Pitter K, LaPlant Q, Hambardzumyan D, Ross BD, Chan TA, Holland EC, Michor F. 2014 Mathematical modeling of PDGF-driven glioblastoma reveals optimized radiation dosing schedules. *Cell* **156**, 603–616. (doi:10.1016/j.cell.2013.12.029)
57. Lenaerts T, Pacheco JM, Traulsen A, Dingli D. 2010 Tyrosine kinase inhibitor therapy can cure chronic myeloid leukemia without hitting leukemic stem cells. *Haematologica* **95**, 900–907. (doi:10.3324/haematol.2009.015271)
58. Sanga S, Sinek JP, Frieboes HB, Ferrari M, Fruehauf JP, Cristini V. 2006 Mathematical modeling of cancer progression and response to chemotherapy. *Expert Rev. Anticancer Ther.* **6**, 1361–1376. (doi:10.1586/14737140.6.10.1361)
59. Sherratt JA, Nowak MA. 1992 Oncogenes, anti-oncogenes and the immune response to cancer: a mathematical model. *Proc. R. Soc. Lond. B* **248**, 261–271. (doi:10.1098/rspb.1992.0071)
60. Kim Y, Lee D, Lee J, Lee S, Lawler S. 2019 Role of tumor-associated neutrophils in regulation of tumor growth in lung cancer development: a mathematical model. *PLoS ONE* **14**, 1–40. (doi:10.1371/journal.pone.0211041)
61. Powell DR, Huttenlocher A. 2016 Neutrophils in the tumor microenvironment. *Trends Immunol.* **37**, 41–52. (doi:10.1016/j.it.2015.11.008)
62. Yan B *et al.* 2013 IL-6 cooperates with G-CSF to induce protumor function of neutrophils in bone marrow by enhancing STAT3 activation. *J. Immunol.* **190**, 5882–5893. (doi:10.4049/jimmunol.1201881)
63. Serizawa M, Takahashi T, Yamamoto N, Koh Y. 2013 Combined treatment with erlotinib and a transforming growth factor-β type I receptor inhibitor effectively suppresses the enhanced motility of erlotinib-resistant non-small-cell lung cancer cells. *J. Thorac. Oncol.* **8**, 259–269. (doi:10.1097/JTO.0b013e318279e942)
64. Deng L, Liang H, Xu M, Yang X, Burnette B, Arina A, Li XD, Mauceri H, Beckett M, Darga T, Huang X. 2014 STING-dependent cytosolic DNA sensing promotes radiation-induced type I interferon-dependent antitumor immunity in immunogenic tumors. *Immunity* **41**, 843–852. (doi:10.1016/j.immuni.2014.10.019)
65. Steinbach KH *et al.* 1979 Estimation of kinetic parameters of neutrophilic, eosinophilic, and basophilic granulocytes in human blood. *Blut* **39**, 27–38. (doi:10.1007/BF01008072)
66. Dale DC, Liles WC, Llewellyn C, Rodger E, Price TH. 1998 Neutrophil transfusions: kinetics and functions of neutrophils mobilized with granulocyte-colony-stimulating factor and dexamethasone. *Transfusion* **38**, 713–721. (doi:10.1046/j.1537-2995.1998.38898375509.x)
67. Kim Y, Wallace J, Li F, Ostrowski M, Friedman A. 2010 Transformed epithelial cells and fibroblasts/myofibroblasts interaction in breast tumor: a mathematical model and experiments. *J. Math. Biol.* **61**, 401–421. (doi:10.1007/s00285-009-0307-2)
68. Kim Y, Friedman A. 2010 Interaction of tumor with its microenvironment: a mathematical model. *Bull. Math. Biol.* **72**, 1029–1068. (doi:10.1007/s11538-009-9481-z)
69. Kim Y, Othmer HG. 2013 A hybrid model of tumor-stromal interactions in breast cancer. *Bull. Math. Biol.* **75**, 1304–1350. (doi:10.1007/s11538-012-9787-0)
70. Salmon P, Le Cotonnec JY, Galazka A, Abdul-AhadA A, Darragh A. 1996 Pharmacokinetics and pharmacodynamics of recombinant human interferon-β in healthy male volunteers. *J. Interferon Cytokine Res.* **16**, 759–764. (doi:10.1089/jir.1996.16.759)
71. Dhooge A, Govaerts W, Kuznetsov YA. 2004 MATCONT: a Matlab package for numerical bifurcation analysis of ODEs. *SIGSAM Bull.* **38**, 21–22. (doi:10.1145/980175.980184)
72. Swan GW. 1988 General applications of optimal control theory in cancer chemotherapy. *Math. Med. Biol.: A J. IMA* **5**, 303–316. (doi:10.1093/imammb/5.4.303)
73. Fister KR, Panetta JC. 2003 Optimal control applied to competing chemotherapeutic cell-kill strategies. *SIAM J. Appl. Math.* **63**, 1954–1971. (doi:10.1137/S0036139902413489)
74. Glick AE, Mastroberardino A. 2017 An optimal control approach for the treatment of solid tumors with angiogenesis inhibitors. *Mathematics* **5**, 49. (doi:10.3390/math5040049)
75. de Pillis LG, Fister KR, Gu W, Head T, Maples K, Neal T, Murugan A, Kozai K. 2008 Optimal control of mixed immunotherapy and chemotherapy of tumors. *J. Biol. Syst.* **16**, 51–80. (doi:10.1142/S0218339008002435)
76. de Pillis LG, Gu W, Fister KR, Head TA, Maples K, Murugan A, Neal T, Yoshida K. 2007 Chemotherapy for tumors: an analysis of the dynamics and a study of quadratic and linear optimal controls. *Math. Biosci.* **209**, 292–315. (doi:10.1016/j.mbs.2006.05.003)
77. Malinzi J, Ouifki R, Eladdadi A, Torres DFM, White KAJ. 2018 Enhancement of chemotherapy using oncolytic virotherapy: mathematical and optimal control analysis. *Math. Biosci. Eng.* **15**, 1435–1463. (doi:10.3934/mbe.2018066)
78. Sabir S, Raissi N, Serhani M. 2020 Chemotherapy and immunotherapy for tumors: a study of quadratic optimal control. *Int. J. Appl. Comput. Math.* **6**, 81. (doi:10.1007/s40819-020-00838-x)
79. Sharma S, Samanta GP. 2016 Analysis of the dynamics of a tumor–immune system with chemotherapy and immunotherapy and quadratic optimal control. *Differ. Equ. Dyn. Syst.* **24**, 149–171. (doi:10.1007/s12591-015-0250-1)
80. Elmouki I, Saadi S. 2016 BCG immunotherapy optimization on an isoperimetric optimal control problem for the treatment of superficial bladder cancer. *Int. J. Dyn. Control* **4**, 339–345. (doi:10.1007/s40435-014-0106-5)
81. Elmouki I, Saadi S. 2016 Quadratic and linear controls developing an optimal treatment for the use of BCG immunotherapy in superficial bladder cancer. *Opt. Control Appl. Methods* **37**, 176–189. (doi:10.1002/oca.2161)
82. Hamdache A, Elmouki I, Saadi S. 2014 Optimal control with an isoperimetric constraint applied to cancer immunotherapy. *Int. J. Comput. Appl.* **94**, 31–37. (doi:10.5120/16421-6073)
83. Fleming WH, Rishel RW. 1975 *Deterministic and stochastic optimal control*, vol. 1, Stochastic modelling and applied probability, 1st edn. New York, NY: Springer.
84. Pontryagin LS. 1987 *Mathematical theory of optimal processes*. Classics of Soviet Mathematics. London, UK: Routledge Taylor & Francis.
85. Hackbusch W. 1978 A numerical method for solving parabolic equations with opposite orientations. *Computing* **20**, 229–240. (doi:10.1007/BF02251947)
86. McAsey M, Mou L, Han W. 2012 Convergence of the forward-backward sweep method in optimal control. *Comput. Optim. Appl.* **53**, 207–226. (doi:10.1007/s10589-011-9454-7)
87. Lenhart S, Workman JT. 2007 *Optimal control applied to biological models*. Mathematical and Computational Biology. New York, NY: Chapman and Hall/CRC.
88. Jonasch E, Haluska FG. 2001 Interferon in oncological practice: review of interferon biology, clinical applications, and toxicities. *Oncologist* **6**, 34–55. (doi:10.1634/theoncologist.6-1-34)
89. Tavakoli M, Manshadi SMP, Naderi N, Dehghan A, Azizi S. 2012 Unusual side effects of interferon Beta-1a in patient with multiple sclerosis. *Mater. Sociomed.* **24**, 203–205. (doi:10.5455/msm.2012.24.203-205)
90. de los Reyes V A, Jung E, Kim Y. 2015 Optimal control strategies of eradicating invisible glioblastoma cells after conventional surgery. *J. R. Soc. Interface* **12**, 20141392. (doi:10.1098/rsif.2014.1392)

91. Jung E, Pumares KJA, Kim Y. 2019 Strategies in regulating glioblastoma signaling pathways and anti-invasion therapy. *PLoS ONE* **14**, e0215547. (doi:10.1371/journal.pone.0215547)
92. Lee J, Lee D, Kim Y. 2021 Mathematical model of STAT signalling pathways in cancer development and optimal control approaches. *R. Soc. Open Sci.* **8**, 210594. (doi:10.1098/rsos.210594)
93. Grimes M *et al.* 2018 Integration of protein phosphorylation, acetylation, and methylation data sets to outline lung cancer signaling networks. *Sci. Signal* **11**, pii. eaaq1087. (doi:10.1126/scisignal.aaq1087)
94. Hattar K *et al.* 2014 Interactions between neutrophils and non-small cell lung cancer cells-enhancement of tumor proliferation and inflammatory mediator synthesis. *Cancer Immunol. Immunother.* **63**, 1297–306. (doi:10.1007/s00262-014-1606-z)
95. Moroy G, Alix AJ, Sapi J, Homebeck W, Bourguet E. 2012 Neutrophil elastase as a target in lung cancer. *Anticancer Agents Med. Chem.* **12**, 565–79. (doi:10.2174/18715201280 0617696)
96. Gong L *et al.* 2013 Promoting effect of neutrophils on lung tumorigenesis is mediated by CXCR2 and neutrophil elastase. *Mol. Cancer* **12**, 154. (doi:10.1186/1476-4598-12-154)
97. Aktas ON, Ozturk AB, Erman B, Erus S, Tanju S, Dilege S. 2018 Role of natural killer cells in lung cancer. *J. Cancer Res. Clin. Oncol.* **144**, 997–1003. (doi:10.1007/s00432-018-2635-3)
98. Yoon H, Tang CM, Banerjee S, Delgado AL, Yebra M, Davis J, Sicklick JK. 2021 TGF-beta-mediated transition of resident fibroblasts to cancer-associated fibroblasts promotes cancer metastasis in gastrointestinal stromal tumor. *Oncogenesis* **10**, 13. (doi:10.1038/s41389-021-00302-5)
99. Sahai E *et al.* 2020 A framework for advancing our understanding of cancer-associated fibroblasts. *Nat. Rev. Cancer* **20**, 174–186. (doi:10.1038/s41568-019-0238-1)
100. Kim Y, Stolarska M, Othmer HG. 2011 The role of the microenvironment in tumor growth and invasion. *Prog. Biophys. Mol. Biol.* **106**, 353–379. (doi:10.1016/j.pbiomolbio.2011.06.006)
101. Eisenberg M, Kim Y, Li R, Ackerman WE, Kniss DA, Friedman A. 2011 Modeling the effects of myoferlin on tumor cell invasion. *Proc. Natl Acad. Sci. USA* **108**, 20 078–20 083. (doi:10.1073/pnas.1116327108)
102. Lee B, Konen J, Wilkinson S, Marcus AI, Jiang Y. 2017 Local alignment vectors reveal cancer cell-induced ECM fiber remodeling dynamics. *Sci. Rep.* **7**, 39498. (doi:10.1038/srep39498)
103. Kim Y, Lawler S, Nowicki MO, Chiocca EA, Friedman A. 2009 A mathematical model of brain tumor: pattern formation of glioma cells outside the tumor spheroid core. *J. Theo. Biol.* **260**, 359–371. (doi:10.1016/j.jtbi.2009.06.025)
104. Revels SL, Lee JM. 2018 Anti-angiogenic therapy in nonsquamous non-small cell lung cancer (NSCLC) with tyrosine kinase inhibition (TKI) that targets the VEGF receptor (VEGFR): perspective on phase III clinical trials. *J. Thorac. Dis.* **10**, 617–620. (doi:10.21037/jtd.2018.01.105)
105. Qu J, Zhang Y, Chen X, Yang H, Zhou C, Yang N. 2017 Newly developed anti-angiogenic therapy in non-small cell lung cancer. *Oncotarget* **9**, 10 147–10 163. (doi:10.18632/oncotarget.23755)
106. Stratigos M, Matikas A, Voutsina A, Mavroudis D, Georgoulias V. 2016 Targeting angiogenesis in small cell lung cancer. *Transl. Lung Cancer Res.* **5**, 389–400. (doi:10.21037/tlcr.2016.08.04)
107. Siegelin MD, Borczuk AC. 2014 Epidermal growth factor receptor mutations in lung adenocarcinoma. *Lab Invest.* **94**, 129–137. (doi:10.1038/labinvest.2013.147)
108. Liu X, Wang WP, Zhang C, Ma Z. 2017 Epidermal growth factor receptor (EGFR): a rising star in the era of precision medicine of lung cancer. *Oncotarget* **8**, 50 209–50 220. (doi:10.18632/oncotarget.16854)
109. Pyonteck SM *et al.* 2013 CSF-1R inhibition alters macrophage polarization and blocks glioma progression. *Nat. Med.* **19**, 1264–1272. (doi:10.1038/nm.3337)
110. Li P, Lu M, Shi J, Hua L, Gong Z, Li Q, Shultz LD, Ren G. 2020 Dual roles of neutrophils in metastatic colonization are governed by the host NK cell status. *Nat. Commun.* **11**, 4387. (doi:10.1038/s41467-020-18125-0)
111. Spiegel A *et al.* 2016 Neutrophils suppress intraluminal NK cell-mediated tumor cell clearance and enhance extravasation of disseminated carcinoma cells. *Cancer Discov.* **6**, 630–49. (doi:10.1158/2159-8290.CD-15-1157)
112. Grauel AL *et al.* 2020 TGFβ-blockade uncovers stromal plasticity in tumors by revealing the existence of a subset of interferon-licensed fibroblasts. *Nat. Commun.* **11**, 6315. (doi:10.1038/s41467-020-19920-5)
113. Broad RV, Jones SJ, Teske MC, Wastall LM, Hanby AM, Thorne JL, Hughes TA. 2021 Inhibition of interferon-signalling halts cancer-associated fibroblast-dependent protection of breast cancer cells from chemotherapy. *Br. J. Cancer* **124**, 1110–1120. (doi:10.1038/s41416-020-01226-4)
114. Liu T, Han C, Wang S, Fang P, Ma Z, Xu L, Yin R. 2019 Cancer-associated fibroblasts: an emerging target of anti-cancer immunotherapy. *J. Hematol. Oncol.* **12**, 86. (doi:10.1186/s13045-019-0770-1)
115. Cho C *et al.* 2020 Cancer-associated fibroblasts downregulate type I interferon receptor to stimulate intratumoral stromagenesis. *Oncogene* **39**, 6129–6137. (doi:10.1038/s41388-020-01424-7)
116. Lee J, Lee D, Lawler S, Kim Y. 2021 Role of neutrophil extracellular traps in regulation of lung cancer invasion and metastasis: structural insights from a computational model. *PLoS Comput. Biol.* **17**, e1008257. (doi:10.1371/journal.pcbi.1008257)
117. Houghton AM *et al.* 2010 Neutrophil elastase-mediated degradation of IRS-1 accelerates lung tumor growth. *Nat. Med.* **16**, 219–223. (doi:10.1038/nm.2084)
118. Sangaletti S *et al.* 2014 Defective stromal remodeling and neutrophil extracellular traps in lymphoid tissues favor the transition from autoimmunity to lymphoma. *Cancer Discov.* **4**, 110–129. (doi:10.1158/2159-8290.CD-13-0276)
119. Uribe-Querol E, Rosales C. 2015 Neutrophils in cancer: two sides of the same coin. *J. Immunol. Res.* **2015**, 983698. (doi:10.1155/2015/983698)
120. Park J *et al.* 2016 Cancer cells induce metastasis-supporting neutrophil extracellular DNA traps. *Sci. Transl. Med.* **8**, 361ra138. (doi:10.1126/scitranslmed.aag1711)
121. Fares J, Fares MY, Khachfe HH, Salhab HA, Fares Y. 2020 Molecular principles of metastasis: a hallmark of cancer revisited. *Signal Transduct. Target Ther.* **5**, 28. (doi:10.1038/s41392-020-0134-x)
122. Das A, Monteiro M, Barai A, Kumar S, Sen S. 2017 MMP Proteolytic activity regulates cancer invasiveness by modulating integrins. *Sci. Rep.* **7**, 14219. (doi:10.1038/s41598-017-14340-w)
123. Arelaki S *et al.* 2016 Gradient infiltration of neutrophil extracellular traps in colon cancer and evidence for their involvement in tumour growth. *PLoS ONE* **11**, e0154484. (doi:10.1371/journal.pone.0154484)
124. Cools-Lartigue J, Spicer J, Najmeh S, Ferri L. 2014 Neutrophil extracellular traps in cancer progression. *Cell Mol. Life Sci.* **71**, 4179–4194. (doi:10.1007/s00018-014-1683-3)
125. Demers M, Wagner DD. 2013 Neutrophil extracellular traps: a new link to cancer-associated thrombosis and potential implications for tumor progression. *Oncoimmunology* **2**, e22946. (doi:10.4161/onci.22946)
126. Wculek SK, Malanchi I. 2015 Neutrophils support lung colonization of metastasis-initiating breast cancer cells. *Nature* **528**, 413–417. (doi:10.1038/nature16140)
127. Tohme S *et al.* 2016 Neutrophil extracellular traps promote the development and progression of liver metastases after surgical stress. *Cancer Res.* **76**, 1367–1380. (doi:10.1158/0008-5472.CAN-15-1591)
128. Aspirin AP, Kim Y. 2020 Polytherapeutic strategies with oncolytic virus-bortezomib and adjuvant NK cells in cancer treatment. *J. R. Soc. Interface* **18**, 20200669. (doi:10.1098/rsif.2020.0669)
129. Göllmann L, Maurer H. 2018 Optimal control problems with time delays: two case studies in biomedicine. *Math. Biosci. Eng.* **15**, 1137–1154. (doi:10.3934/mbe.2018051)
130. Ledzewicz U, Wang S, Schättler H, André N, Heng MA, Pasquier E. 2017 On drug resistance and metronomic chemotherapy: a mathematical modeling and optimal control approach. *Math. Biosci. Eng.* **4**, 217–235. (doi:10.3934/mbe.2017014)
131. Rihan FA, Lakshmanan S, Maurer H. 2019 Optimal control of tumour-immune model with time-delay and immuno-chemotherapy. *Appl. Math. Comput.* **353**, 147–165. (doi:10.1016/j.amc.2019.02.002)
132. Rodríguez CR, Calvo GF, Ramis-Conde I, Belmonte-Beitia J. 2017 Stochastic modelling of slow-progressing tumors: analysis and applications to the cell interplay and control of low grade gliomas. *Commun. Nonlinear Sci. Numer. Simul.* **49**, 63–80. (doi:10.1016/j.cnsns.2017.02.008)
133. Schättler H, Ledzewicz U. 2015 Optimal control for mathematical models of cancer therapies. In *An application of geometric methods*. New York, NY: Springer.
134. Ledzewicz U, Brown T, Schättler H. 2004 Comparison of optimal controls for a model in

cancer chemotherapy with L1- and L2-type objectives. *Optim. Methods Softw.* **19**, 339–350. (doi:10.1080/10556780410001683104)

135. Amulic B, Cazalet C, Hayes GL, Metzler KD, Zychlinsky A. 2012 Neutrophil function: from mechanisms to disease. *Annu. Rev. Immunol.* **30**, 459–489. (doi:10.1146/annurev-immunol-020711-074942)
136. Xu Y *et al.* 2013 Cigarette smoke (CS) and nicotine delay neutrophil spontaneous death via suppressing production of diphosphoinositol pentakisphosphate. *Proc. Natl Acad. Sci. USA* **110**, 7726–7731. (doi:10.1073/pnas.1302906110)
137. Kasahara Y, Iwai K, Yachie A, Ohta K, Konno A, Seki H, Miyawaki T, Taniguchi N. 1997 Involvement of reactive oxygen intermediates in spontaneous and CD95 (Fas/APO-1)-mediated apoptosis of neutrophils. *Blood* **89**, 1748–1753. (doi:10.1182/blood.V89.5.1748)
138. Dibbert B, Weber M, Nikolaizik WH, Vogt P, Schöni MH, Blaser K, Simon HU. 1999 Cytokine-mediated Bax deficiency and consequent delayed neutrophil apoptosis: a general mechanism to accumulate effector cells in inflammation. *Proc. Natl Acad. Sci. USA* **96**, 13 330–13 335. (doi:10.1073/pnas.96.23.13330)
139. Gabelloni ML, Trevani AS, Sabatte J, Geffner J. 2013 Mechanisms regulating neutrophil survival and cell death. *Semin. Immunopathol.* **35**, 423–437. (doi:10.1007/s00281-013-0364-x)
140. Ibrahim SA, Kulshrestha A, Katara GK, Beaman KD. 2017 Delayed neutrophil apoptosis is regulated by cancer associated a2 isoform vacuolar ATPase. *J. Immunol.* **198**(1 Suppl), 76.15.
141. Kuijpers T, Lutter R. 2012 Inflammation and repeated infections in CGD: two sides of a coin. *Cell Mol. Life Sci.* **69**, 7–15. (doi:10.1007/s00018-011-0834-z)
142. Takeshima T, Pop LM, Laine A, Iyengar P, Hannan ESVR. 2016 Key role for neutrophils in radiation-induced antitumor immune responses: potentiation with G-CSF. *Proc. Natl Acad. Sci. USA* **113**, 11 300–11 305. (doi:10.1073/pnas.1613187113)
143. Andzinski L, Wu CF, Lienenklaus S, Kroger A, Weiss S, Jablonska J. 2015 Delayed apoptosis of tumor associated neutrophils in the absence of endogenous IFN-β. *Int. J. Cancer* **136**, 572–583. (doi:10.1002/ijc.28957)
144. Basin M, Rodriguez-Gonzalez J, Martinez-Zuniga R. 2004 Optimal control for linear systems with time delay in control input. *J. Franklin Inst.* **341**, 267–278. (doi:10.1016/j.jfranklin.2003.12.004)
145. Forde JE, Ciupe SM, Cintron-Arias A, Lenhart S. 2016 Optimal control of drug therapy in a hepatitis B model. *Appl. Sci.* **6**, 219. (doi:10.3390/app6080219)
146. Jean-Quartier C, Jeanquartier F, Jurisica I, Holzinger A. 2018 In silico cancer research towards 3R. *BMC Cancer* **18**, 408. (doi:10.1186/s12885-018-4302-0)
147. Vermolen FJ, van der Meijden RP, van Es M, Gefen A, Weihs D. 2015 Towards a mathematical formalism for semi-stochastic cell-level computational modeling of tumor initiation. *Ann. Biomed. Eng.* **43**, 1680–1694. (doi:10.1007/s10439-015-1271-1)
148. Aguda BD, Kim Y, Hunter MG, Friedman A, Marsh CB. 2008 MicroRNA regulation of a cancer network: consequences of the feedback loops involving miR-17-92, E2F, and Myc. *Proc. Natl Acad. Sci. USA* **105**, 19 678–19 683. (doi:10.1073/pnas.0811166106)
149. Jenner AL, Kim PS, Frascoli F. 2019 Oncolytic virotherapy for tumours following a Gompertz growth law. *J. Theor. Biol.* **480**, 129–140. (doi:10.1016/j.jtbi.2019.08.002)
150. Aguda BD, Kim Y, Kim HS, Friedman A, Fine H. 2011 Qualitative network modeling of the MYC-p53 control system of cell proliferation and differentiation. *Biophys. J.* **101**, 2082–2091. (doi:10.1016/j.bpj.2011.09.052)
151. Aspirin AP, Kim Y. 2021 Polytherapeutic strategies with oncolytic virus-bortezomib and adjuvant NK cells in cancer treatment. *J. R. Soc. Interface* **18**, 20200669. (doi:10.1098/rsif.2020.0669)
152. Reyes AAVL, Jung E, Kim Y. 2015 Optimal control strategies of eradicating invisible glioblastoma cells after conventional surgery. *J. R. Soc. Interface* **12**, 20141392. (doi:10.1098/rsif.2014.1392)
153. Villasana M, Radunskaya A. 2003 A delay differential equation model for tumor growth. *J. Math. Biol.* **47**, 270–94. (doi:10.1007/s00285-003-0211-0)
154. Bernabeu MO *et al.* 2020 Abnormal morphology biases hematocrit distribution in tumor vasculature and contributes to heterogeneity in tissue oxygenation. *Proc. Natl Acad. Sci. USA* **117**, 27 811–27 819. (doi:10.1073/pnas.2007770117)
155. Friedman A, Kim Y. 2011 Tumor cells proliferation and migration under the influence of their microenvironment. *Math. Biosci. Eng.* **8**, 373–385.
156. Kim Y, Boushaba K. 2011 An enzyme kinetics model of tumor dormancy, regulation of secondary metastases. *Discrete Continuous Dyn. Syst.-S* **4**, 1465–1498. (doi:10.3934/dcdss.2011.4.1465)
157. Kim Y, Roh S, Lawler S, Friedman A. 2011 miR451 and AMPK/MARK mutual antagonism in glioma cells migration and proliferation. *PLoS ONE* **6**, e28293. (doi:10.1371/journal.pone.0028293)
158. Kim Y, Lee HG, Dmitrieva N, Kim J, Kaur B, Friedman A. 2014 Choindroitinase ABC I-mediated enhancement of oncolytic virus spread and anti-tumor efficacy: a mathematical model. *PLoS ONE* **9**, e102499. (doi:10.1371/journal.pone.0102499)
159. Kim Y, Lee J, Lee D, Othmer HG. 2019 Synergistic effects of bortezomib-OV therapy and anti-invasive strategies in glioblastoma: a mathematical model. *Cancers* **11**, 215. (doi:10.3390/cancers11020215)
160. Lee HG, Kim Y. 2016 The role of the microenvironment in regulation of CSPG-driven invasive and non-invasive tumor growth in glioblastoma. *Japan J. Indust. Appl. Math.* **32**, 771–805. (doi:10.1007/s13160-015-0188-2)
161. Lee W, Lim S, Kim Y. 2017 The role of myosin II in glioma invasion: a mathematical model. *PLoS ONE* **12**, e0171312. (doi:10.1371/journal.pone.0171312)
162. Rejniak K. 2007 An immersed boundary framework for modelling the growth of individual cells: an application to the early tumour development. *J. Theor. Biol.* **247**, 186–204. (doi:10.1016/j.jtbi.2007.02.019)
163. Macklin P, Edgerton ME, Thompson AM, Cristini V. 2012 Patient-calibrated agent-based modelling of ductal carcinoma in situ (DCIS): from microscopic measurements to macroscopic predictions of clinical progression. *J. Theor. Biol.* **301**, 122–140. (doi:10.1016/j.jtbi.2012.02.002)
164. Lambert B, MacLean AL, Fletcher AG, Combes AN, Little MH, Byrne HM. 2018 Bayesian inference of agent-based models: a tool for studying kidney branching morphogenesis. *J. Math. Biol.* **76**, 1673–1697. (doi:10.1007/s00285-018-1208-z)
165. Drasdo D, Hohme S. 2005 A single-cell-based model of tumor growth in vitro: monolayers and spheroids. *Phys. Biol.* **2**, 133–147. (doi:10.1088/1478-3975/2/3/001)
166. Kim Y, Lee D, Lawler S. 2020 Collective invasion of glioma cells through OCT1 signalling and interaction with reactive astrocytes after surgery. *Phil. Trans. R. Soc. B* **375**, 20190390. (doi:10.1098/rstb.2019.0390)
167. Damaghi M *et al.* 2021 The harsh microenvironment in early breast cancer selects for a Warburg phenotype. *Proc. Natl Acad. Sci. USA* **118**, e2011342118. (doi:10.1073/pnas.2011342118)
168. Rejniak KA, Anderson ARA. 2011 Hybrid models of tumor growth. *WIRES Syst. Biol. Med.* **3**, 115–125. (doi:10.1002/wsbm.102)
169. Kim Y, Stolarska M, Othmer HG. 2007 A hybrid model for tumor spheroid growth in vitro I: theoretical development and early results. *Math. Models Methods Appl. Sci.* **17**, 1773–1798. (doi:10.1142/S0218202507002479)
170. Kim Y. 2013 Regulation of cell proliferation and migration in glioblastoma: new therapeutic approach. *Front. Mol. Cellular Oncol.* **3**, 53. (doi:10.3389/fonc.2013.00053)
171. Kim Y, Roh S. 2013 A hybrid model for cell proliferation and migration in glioblastoma. *Discrete Continuous Dyn. Syst.-B* **18**, 969–1015. (doi:10.3934/dcdsb.2013.18.969)
172. Kim Y, Othmer H. 2015 Hybrid models of cell and tissue dynamics in tumor growth. *Math. Biosci. Eng.* **12**, 1141–1156. (doi:10.3934/mbe.2015.12.1141)
173. Kim Y, Powathil G, Kang H, Trucu D, Kim H, Lawler S, Chaplain M. 2015 Strategies of eradicating glioma cells: a multi-scale mathematical model with miR-451-AMPK-mTOR control. *PLoS ONE* **10**, e0114370. (doi:10.3389/fonc.2013.00053)
174. Metzcar J, Wang Y, Heiland R, Macklin P. 2019 A review of cell-based computational modeling in cancer biology. *JCO Clin. Cancer Inform.* **3**, 1–13. (doi:10.1200/CCI.18.00069)
175. Stolarska M, Kim Y, Othmer HG. 2009 Multiscale models of cell and tissue dynamics. *Phil. Trans. R. Soc. A* **367**, 3525–3553. (doi:10.1098/rsta.2009.0095)
176. Kim Y, Kang H, Powathil G, Kim H, Trucu D, Lee W, Lawler S, Chaplain M. 2018 Role of extracellular matrix and microenvironment in regulation of tumor growth and LAR-mediated invasion in glioblastoma. *PLoS ONE* **13**, e0204865. (doi:10.1371/journal.pone.0204865)